2012

A Multifaceted Approach Identifies ErbB2 and ErbB3 proteins and microRNA-125b as Key Contributors to Prostate Cancer Progression

Danielle Weaver
Virginia Commonwealth University

A Multifaceted Approach Identifies ErbB2 and ErbB3 proteins and microRNA-125b as

Key Contributors to Prostate Cancer Progression

A thesis submitted in partial fulfillment of the requirements for the degree of Master of Science

in Bioinformatics at Virginia Commonwealth University.

by

Danielle Elizabeth Weaver,

BS Forensic Science

Virginia Commonwealth University December, 2009

Director: Zendra Zehner, PhD,

Department of Biochemistry and Molecular Biology

Virginia Commonwealth University

Richmond, Virginia

May, 2012

Acknowledgement

The author wishes to thank several people. I would like to thank my mother Maureen and my father Gary for their unwavering support over the past 2 years it has taken me to graduate, as well as the previous 5 or so years it took to achieve my BS degree. I would also like to give many thanks to Dr. Zendra Zehner for taking a chance on me and giving me the opportunity to learn from her, as well as the opportunity to work on this project. I would like to thank my committee members for their input on my project goals and assistance with my writing. I thank Joe Anderson for his help building the prostate specific network. I thank Sarah Seashols for her support and advice both in the lab and out. I thank William Budd for all of his support and advice throughout the past 2 years as well as his help in developing these many projects that eventually became a thesis. Lastly, I thank the NIH/NCI for funding portions of this project.

Abstract

A MULTIFACETED APPROACH IDENTIFIES ERBB2 AND ERBB3 PROTEINS AND

MICRORNA-125B AS KEY CONTRIBUTORS TO PROSTATE CANCER PROGRESSION

by

Danielle E. Weaver, BS

A thesis submitted in partial fulfillment of the requirements for the degree of Master of Science

in Bioinformatics at Virginia Commonwealth University.

Virginia Commonwealth University, 2012

Prostate cancer is the most common cancer affecting men today. Therefore, there is a strong need for accurate biomarkers and successful therapeutic treatments. A novel approach combining a computationally built protein-protein interaction network of proven microRNA protein targets with high throughput proteomics identified ErbB2 and ErbB3 as key proteins in prostate cancer. These results coupled with microRNA array screening of an androgen-independent prostate cancer progression model, substantiated by single microRNA analysis, suggested miR125b as a key tumor suppressor contributing to prostate cancer progression. miR125b expression was shown to be substantially increased in the non-tumorigenic P69 cell line compared to its highly tumorigenic, metastatic M12 variant. Luciferase reporter gene assays including the entire 3'UTR of either ErbB2 or ErbB3 revealed a 2.8- and 2.4-fold decrease (respectively) compared to control vector. Thus, this combinatorial approach has suggested an additional microRNA and its target involved in prostate tumor progression.

Chapter 1: Introduction

The Prostate Organ:

The prostate organ is part of the male reproductive system and is located in front of the rectum and under the bladder. The prostate is an exocrine gland that produces two-thirds of the volume of seminal fluid. This fluid is alkaline in nature to help neutralize the acidity of the vagina, allowing sperm to survive longer and protect genetic material. During ejaculation, the prostate's smooth muscles contract helping to expel the seminal fluid, carrying the sperm through the penis as semen.

A healthy and mature prostate is roughly the size of a walnut and surrounds the urethra, the tube that passes urine from the bladder to the penis. In half of all men, around the age of fifty, the prostate begins to enlarge to abnormal size due to male hormones (androgens). This enlarging of the prostate can be classified as benign growth or malignant. Benign cases are often referred to as benign prostatic hyperplasia (BPH), where the prostate becomes enlarged and presses on the urethra slowing or stopping the flow of urine. This is non-cancerous and the overgrowth of these cells does not result in invasion into other tissue. In malignant cases, the cells can invade or damage nearby tissue leading to cancer of the prostate gland.

Incidence of Prostate Cancer in the United States:

Prostate Cancer is the most common cancer affecting men in the United States today with over 2.5 million identified manifestations [1]. It is the second leading cause of cancer related deaths in American men [2]. In 2012, it is estimated that 241,740 new cases of prostate cancer will

be diagnosed and 28,170 men will succumb to the disease [1]. Essentially one in every six males in the U.S. will develop prostate cancer in their lifetime.

The development of prostate cancer has been linked to age, race, and family history [2]. Age is an important factor influencing the likelihood of contracting the disease. Nearly 65% of men diagnosed with prostate cancer are of age 65 or older. Figure 1-1 depicts the incidence of prostate cancer in all males according to age at the time of diagnosis per 100,000 men based on the data obtained from the National Cancer Institute Surveillance Epidemiology and End Results database[3]. Therefore, a man's risk of developing prostate cancer increases as he ages and peaks between the ages of 70-74. It is remarkably uncommon for men to be diagnosed prior to the age of 50.

In addition to age, a man's race or ethnicity has a major influence on the probability of contracting the disease. On average, 156 out of every 100,000 males in the United States will be diagnosed with prostate cancer [3]. White males have a lower than average overall incidence of prostate cancer of 149.5 out of every 100,000 males. African-American males have the highest overall incidence rate of 233.8 out of every 100,000. Figure 1-2 depicts the incidence of prostate cancer broken down by both age at the time of diagnosis and race/ethnicity per every 100,000 males in the population [4]. African-American men are three times more likely to die from prostate cancer than their white counterparts, while Asian-American men are the least likely race to contract the disease [2].

Family history, as in most diseases, also plays a role in a man's risk for developing prostate cancer. Men who have a single relative who was diagnosed with prostate cancer are twice as likely to develop the disease, while men with two or more relatives who have the

Figure 1-1: Variation in the incidence of prostate cancer based on age of patient.

Age is an important factor influencing the likelihood of contracting the disease. Nearly 65% of men diagnosed with prostate cancer are of age 65 or older [2]. Men are most commonly diagnosed around age 70 and very infrequently diagnosed prior to the age of 50. Incidence is based on 100,000 men.

Figure 1-1: Variation in the incidence of prostate cancer based on age of patient.
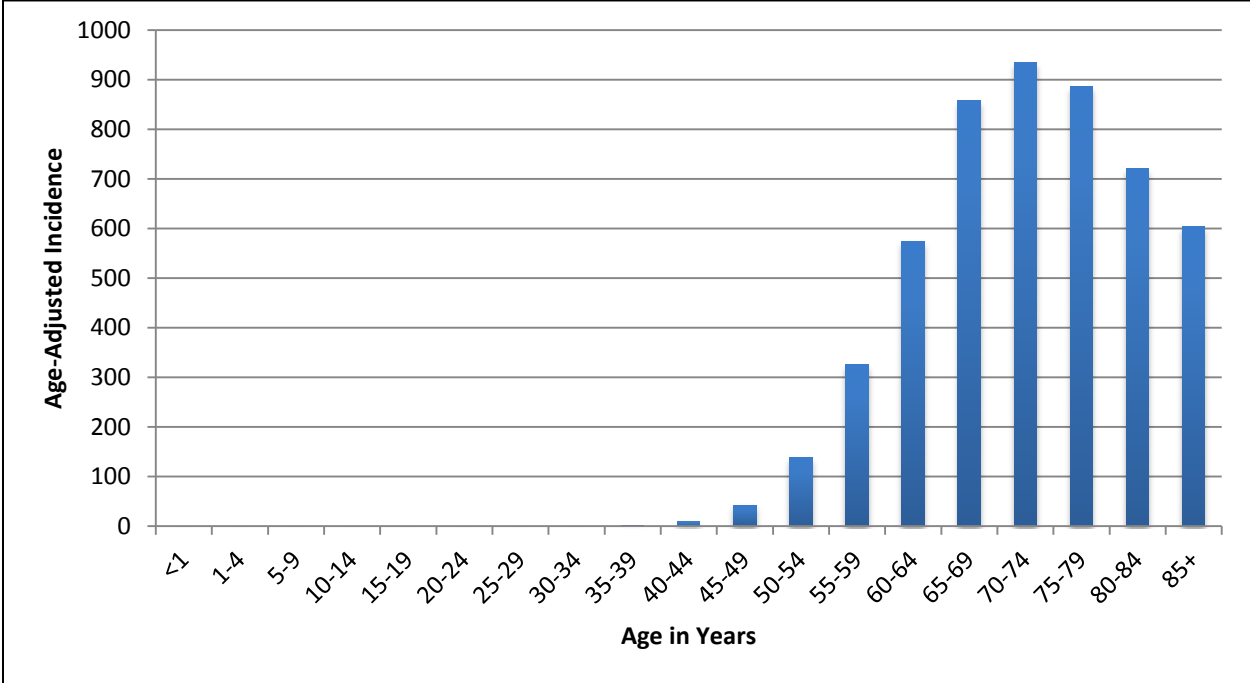
Figure 1-2: Variation in incidence of prostate cancer based on age and race/ethnicity.
African-American males are much more likely to contract prostate cancer than any other race in the United States. Asian-American males are least likely to be diagnosed with the disease. All males are most commonly diagnosed around age 70. Incidence is based on 100,000 men.

Figure 1-2: Variation in incidence of prostate cancer based on age and race/ethnicity.
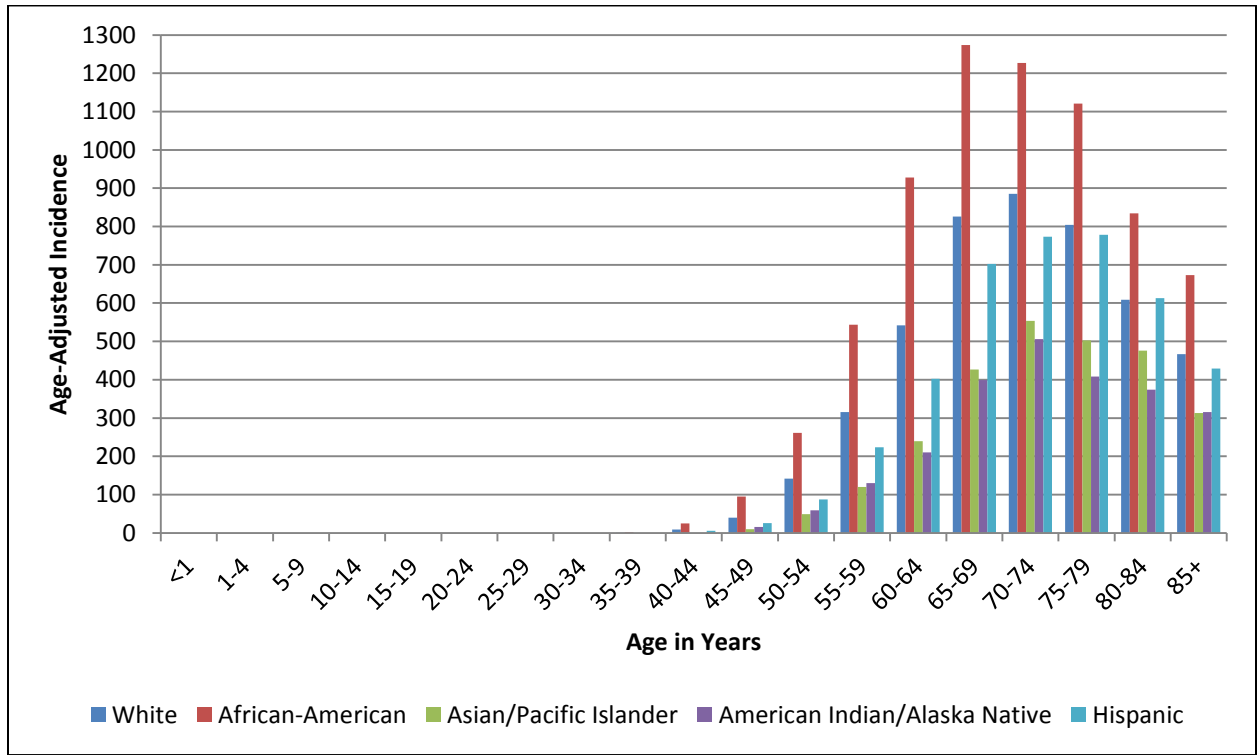
disease are four times as likely[2]. The men who are most susceptible are those whose family members were diagnosed prior to the age of 50 due to the rarity of the disease at younger ages.

Prostate Cancer Detection:

In 1986 the U.S. Food and Drug Administration (FDA) approved the prostate specific antigen (PSA) test for monitoring disease status in prostate cancer patients [5]. In 1994 the FDA approved the PSA test for early detection of prostate cancer in men of age 50 or older. PSA is a protein produced by cells in the prostate gland [6]. The PSA test measures the level of the PSA protein in the blood to determine those at risk for developing the disease. Low levels of PSA are normal while increased levels of PSA can be present for benign or malignant conditions. However, PSA levels alone cannot effectively diagnose prostate cancer, therefore a digital rectal exam (DRE) is used in combination with PSA monitoring for diagnosing the disease. A multi-institute funded clinical trial comparing the PSA test and DRE as screening tools determined that PSA testing alone identified 75% of tumors while DRE only identified 55%[7]. The combination of both the PSA test and DRE test identified the most tumors, 78%.

Figure 1-3 depicts the trend in prostate cancer detection from 1975 to 2008 according to the data provided from the National Cancer Institute Surveillance Epidemiology and End Results database. In 1975, 94 out of every 100,000 men were diagnosed with prostate cancer [3]. Beginning in 1987, exponential growth was seen in the incidence rate, peaking in 1992 with 237 out of every 100,000 men being diagnosed. As of 2008, 153 out of every 100,000 men were diagnosed. Several schools of thought have emerged as to the enormous spike in prostate cancer detection in the late 80's early 90's, with the introduction of PSA testing being on the forefront.

Figure 1-3: Prostate cancer incidence trend 1975-2008.

In 1975, 94 out of every 100,000 men were being diagnosed with prostate cancer. Beginning in 1987, exponential growth was seen in the incidence rate, peaking in 1992 with 237 out of every 100,000 men being diagnosed. As of 2008, 153 out of every 100,000 men are being diagnosed [3].

Figure 1-3: Prostate cancer incidence trend 1975-2008.
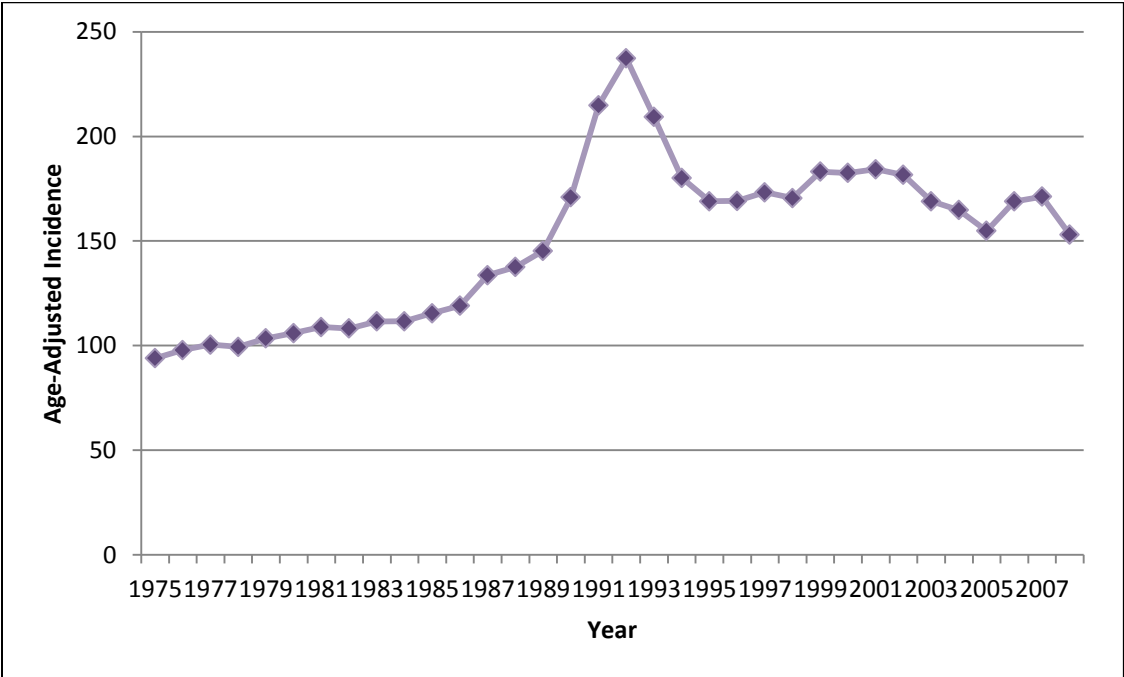
Increased awareness of the disease as well as the fact that the average life span of Americans has increased are also contributing to the increase in detection of prostate cancer.

The genetics of prostate tumorigenesis:

As stated before, genetics and family history can play a major role in the development of prostate cancer. Prostate cancer has a heterogeneous nature and is highly complex therefore mutations in a multitude of genes can play a role in tumor progression [8]. Consequently, scientists are actively trying to identify genes, RNAs and proteins that can be associated with tumor progression and serve potentially as biomarkers. A biomarker is a biological molecule that can be quantified and is associated with normal or better yet abnormal forms of a disease. Table 1-1 shows a list of genes and their associated functions from a recent study identifying differentially-regulated genes from androgen-dependent to androgen-independent tumor progression [8]. Only the most differentially expressed genes were selected; however, these are unquestionably not the only genes associated with prostate tumorigenesis. Genes are thought to influence tumor progression by the accumulation of point mutations that inadvertently inactivate the gene or by dysregulation via several routes.

Tumor reoccurrence emerges in 15-30% of prostate cancer patients generally within 5 years of initial treatment [2]. These patients are then treated with androgen withdraw (AW) therapy and 70-80% of patients respond positively to this treatment temporarily. However, eventually the tumors progress to an androgen-independent, a highly metastatic and aggressive form [9]. In a normal prostate cell and androgen-dependent prostate tumors, testosterone will bind to the androgen receptor triggering the production of androgen transcripts which stimulates cell growth.

Table 1-1: Differentially expressed genes from androgen-dependent to androgen-independent prostate tumor progression.

Gene Symbol	Gene Name	Function	Chromosome location
IGF1	Insulin-like growth factor 1	Involved in mediating growth and development	12q23.2
EGFR/ERBB	Epidermal growth factor receptor	Influences cell proliferation	7p12
TM4SF1	Transmembrane 4 L six family member 1	Plays a role in regulation of cell development, activation, growth and motility.	3q21-q25
WT1	Wilms tumor 1	Plays essential role in normal development of urogenital system	11p13
PAGE-1	P antigen family member 1	Expressed in a variety of tumors but not normal tissue. Function currently unknown	Xp11.23
RAB27B	RAS related protein 27 B	Member of the RAS oncogene family. Involved in vesicular fusion and trafficking	18q21.2
SOX4	SRY- sex determining region Y	Regulates embryonic development. May function in apoptosis as well as tumorigenesis	6p22.3

A study has shown that in cases of androgen-independent tumorigenesis, 50% of the tumors had point mutations in the androgen receptor gene. Scientists are currently unsure of how androgen receptors still promote cell growth in the absence of testosterone, but the point mutations may play a role in this phenomenon.

Fairly recently small non-coding RNAs have been discovered to influence gene expression by either inhibiting translation or signaling the transcribed genetic message (messengerRNA, mRNA) for degradation. One class of responsible small RNAs are known as microRNAs (miRNAs, miRs).

The discovery of miRNAs and their role in oncogenesis:

MicroRNAs are small non-coding RNAs that are 19-25 (nt) in length [10]. They have the ability to post-transcriptionally regulate gene function by inhibiting translation or marking an mRNA for degradation. miRNAs have been shown to influence a variety of biological processes such as cell cycle regulation, differentiation, development, metabolism and aging [10]. miRNAs were discovered in 1993 in *C. elegan* development[10]. They are highly conserved among organisms that are very distantly related such as invertebrates, vertebrates and plants. The miRBase database, a database of published miRNAs with annotations, listed 18,226 identified miRNAs from an assortment of organisms as of November 2011 [11].

miRNAs presumably play a role in cancer due to their natural influence on cell cycle regulation (cell proliferation and apoptosis), differentiation, development and other related biological processes [12, 13]. miRNAs are very frequently located in cancer-related genomic regions such as minimal regions of amplification, loss of heterozygosity, fragile sites, and common break point regions on or near oncogenes or tumor suppressor genes. miRNAs function as either

oncogenes or tumor suppressors. Oncogenes have been shown to be consistently up-regulated in tumor verses normal tissue whereas tumor suppressors are down-regulated in tumor versus normal tissue [10, 12]. It also has been show that in some instances, a miRNA may act as a tumor suppressor in one setting and an oncogene in another [12]. Studies have shown that in some cancers, a global deregulation of miRNAs has been found. This implicates that miRNAs generally target genes associated with biological processes that are critical for development or progression of the disease.

MicroRNA biogenesis and mRNA targeting:

miRNAs have been located in the genome in both introns and exons of coding proteins as well as intergenic regions [12]. It is quite common for them to be found polycistronically, clustered in groups of 2-7 miRNAs as a single transcript controlled by a common regulator, or monocistronically [12, 14]. The first step of miRNA biogenesis begins in the nucleus where the precursor is transcribed by RNA polymerase II, adding a 5' cap and a 3' poly-A tail (Figure 1-4)[10, 12-14]. This pri-miRNA is then cleaved into a 70-100 nt hairpin shaped fragment by a ribonuclease II called Drosha and the double-stranded DNA binding protein DGCR8. The new fragment is referred to as pre-miRNA. After the hairpin structure is formed, the pre-miRNA is exported out into the cytoplasm by means of the nuclear export factor exportin. The pre-miRNA is then processed into a 19-25 nt miRNA duplex via association with the ribonuclease III Dicer. The miRNA is then incorporated into the RNA-induced silencing complex (RISC). The miRNA is now mature and is guided toward its intended mRNA target.

miRNAs target genes via complementarity between the miRNA sequence ("seed" region, bases 2-7 of the miRNA from the 5' end) and the 3'UTR sequence of the mRNA transcript [12, 14].

Figure 1-4: microRNA Biogenesis

1. Within the nucleus, the precursor is transcribed by RNA polymerase II and the 5'cap and 3'poly-A tail is added.

2. Also within the nucleus, the pri-miRNA is cleaved into a 70-100 nt hairpin shaped fragment known as pre-miRNA by Drosha.

3. The pre-miRNA is exported out of the nucleus into the cytoplasm by Exportin.

4. Now in the cytoplasm, the pre-miRNA is processed into a 19-25 nt miRNA duplex by Dicer.

5. The miRNA duplex is incorporated into RISC and one strand selected as the mature miRNA and is now prepared to locate its intended target.

Figure 1-4: Steps in microRNA Biogenesis

gene

1

5' cap

AAAAAAAA

pri-miRNA

Drosha

2

pre-miRNA

3

Nucleus

Cytosol

Exportin

pre-miRNA

Dicer

4

RISC

RISC

5

Mature miRNA 5p/3p
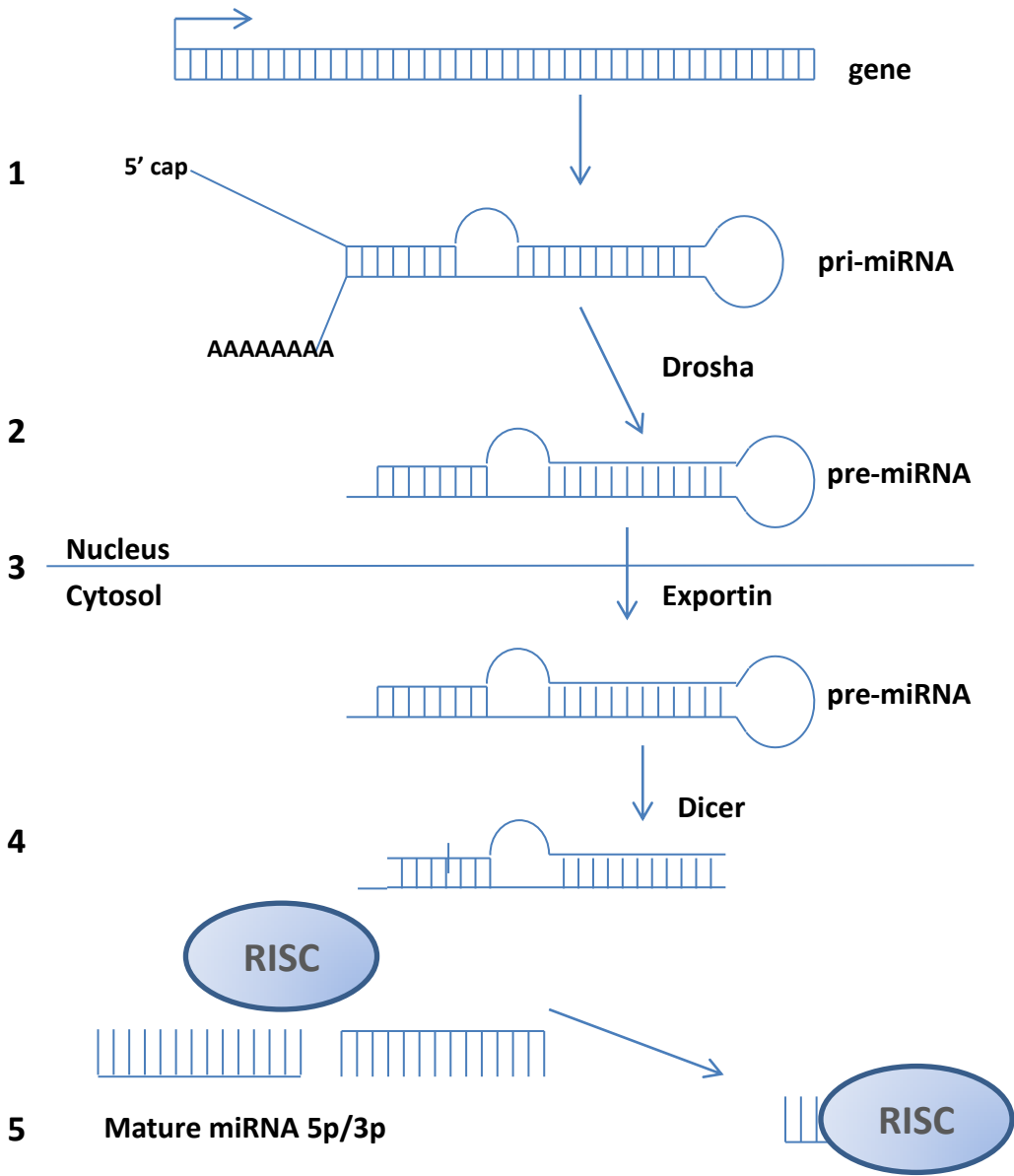
Recently it has been shown that in some cases, a miRNA's seed sequence complementarity will correspond to the 5'UTR of an mRNA transcript or potentially, association with any portion of the target mRNA is sufficient for translational repression [15]. Perfect or near perfect binding complementarity of the miRNA seed region to the target gene leads to mRNA degradation through the RNA-mediated degradation pathway. Imperfect complementarity is thought to lead to translational repression [12] at some step down stream of initiation but the mechanism for this effect remains to be validated [15]. It is estimated that over 30% of protein coding genes are regulated by miRNAs [12]. This along with the fact that the seed region of most miRNAs is around 6 nt in length, it is suggested that miRNAs can regulate multiple protein-coding genes.

The Oncogenic Potential of miR17-3p and miR125b when differentially expressed:

The gene that encodes for the miR17-3p (miR17*) mature miRNA is located on chromosome 13 in a polycistronic cluster known as the miR-17-92 cluster [16]. The cluster is transcribed into a primary transcript that encodes six miRNAs [17]. These include miR17 (miR17-5p and miR17-3p mature miRNAs), miR18a, miR19a, miR20a, miR19b-1 and miR92-1. The cluster has been shown to be activated by the c-MYC transcription factor [18]. In human solid tumors, miR17-5p was shown to be up-regulated in breast, colon, lung, pancreas and prostate cancers [19]. In the same study, miR20a was shown to be up-regulated in colon, pancreas and prostate cancers. miR17-3p has been shown to be down-regulated in prostate cancer when comparing benign versus malignant tumor samples collected via laser capture microdissection [19].

A gene that encodes for the miR125b is located in two separate locations within the human genome, chromosomes 11 and 21 (precursor miR125b_1 and miR125b_2 respectively) both found monocistronically. When fully processed both precursors produce mature miR125b

molecule. miR125b has been shown to be differentially dysregulated in a multitude of human cancers: down-regulated in breast [20, 21], ovarian [22], squamous cell carcinoma [23], but up-regulated in neuroblastoma [24], stomach [25], colon [21], and bladder [26]. According to miRecords, an online database of miRNA-target interactions, miR125b has been experimentally proven to target 52 proteins as of November 2010[27].

Prostate Cancer Cell Models:

There are three classical sets of tissue culture cell lines used by researchers to help better investigate prostate cancer overall and prostate cancer tumor progression. The LNCaP, DU-145, and the P-C3 cell lines [28]. The DU-145 cell line was the first prostate cancer cell line to be established and was derived from a metastatic tumor excised from the brain of a 69 year old white male with prostate cancer. These cells fail to express the androgen receptor gene/protein (AR), therefore classifying them as androgen-independent.

The LNCaP cell line was derived from a biopsy of a lymph node metastasis from a 50 year old white male with prostate cancer [28]. Although there are 60+ LNCaP sublines, the parental cell line expresses both the AR gene and protein, classifying them as androgen-dependent. This is currently the most popular cell line used by researchers.

The PC-3 cell line was derived from a lumbar vertebra metastasis from a 62 year old white male with prostate cancer [28]. The parental cell line fails to express the AR gene/protein, classifying them as androgen-independent. There are 11 sublines that have been derived from the PC-3 parental cell line, some of which are androgen-dependent.

The model system used in our lab is a genetically related androgen-independent cell line derived from a non-neoplastic prostate epithelial cell from a 63 year old African American male

17

[29]. These cells were immortalized with the SV40 Large T Antigen gene and referred to as P69. The P69 cell line is non-metastatic, and weakly tumorigenic. The M12 cell line was derived from the parental P69 line by interperitonal injection into male, athymic nude mice. In some cases after sufficient time (months) tumors developed. Tumors were collected, cells dispersed, and reinjected into mice as before [29]. After three rounds of injections the resulting M12 cell line was derived. The karyotype for the M12 subline shows an unequal translocation of chromosome 16:19, resulting in the loss of most of one copy of chromosome 19. Interestingly, an independently derived second cell line showed a similar chromosomal rearrangement as the M12 cell line suggesting this chromosomal rearrangement can be independently duplicated during tumorigenesis. The M12 cell line is highly metastatic and tumorigenic when injected orthtopically into male, athymic nude mice. The F6 subline was derived from the M12 cell line by restoration of the lost copy of chromosome 19 via micro-cell fusion techniques [30]. The restoration of the second copy of chromosome19 resulted in a poorly tumorigenic, non-metastatic phenotype for the F6 cell line, like the P69 predecessor. Altogether, these cell lines generate a useful model system for studying factors that contribute to the progression from a normal epithelial cell line to a highly metastatic, tumorigenic versus weakly variant, originally derived from a common cellular background.

Previously, it was found that the P69 cell line had a relatively high abundance of the human miRNA 17-3p. The M12 subline exhibits a two-fold decrease in the expression of miR17-3p compared to the parental P69 cell line. A M12 subline with restored expression (approximate an additional 3-fold) of miR17-3p (M12+miR17-3p) was derived [31]. A variety of experiments suggests that miR17-3p acts as tumor suppressor *in vitro* and *in vivo* [31].

The ErbB Protein family and it's role in oncogenesis:

The the ErbB family or epidermal growth factor receptor (EGFR) family is comprised of four protein homologs: EGFR/ErbB1/HER1, ErbB2/HER2/Neu, ErbB3/HER3 and ErbB4/HER4 [32]. All of these members are type 1 transmembrane tyrosine kinase receptors and contain a extracellular ligand-binding domain, a single transmembrane-spanning region and a cytoplasmic protein tyrosine kinase domain attached to a C-terminal tail [2]. Signaling by the ErbB family has been shown to regulate several cellular activities including cell division, migration, adhesion, differentiation and apoptosis.

The ErbB receptors are activated by mesenchymal ligands to include heregulines, neureguins and other EGF-like ligands, each with an EGF-like domain for binding specificity [32]. When a ligand binds to the extracellular ligand-binding domain, it activates the ErbB receptor allowing dimerization to another ligand-bound ErbB receptor[2]. This is true for all members except for ErbB2 which is constitutively available for dimerization, thus not requiring ligand binding for activation [32].

The ErbB receptors can either homo or hetero dimerize and this action is essential to their function and signaling activity [2]. Homodimers only propagate a weak signal compared to heterodimers. ErbB2 has been shown to be the primary heterodimerization partner for all other ErbB members [32] and ErbB2 heterodimers are the most potent [2]. ErbB3 is unable to homodimerize due to insufficient kinase signaling but ErbB2-ErbB3 heterodimers are the most mitogenic of all of the other heterodimer combinations. ErbB4 expression has been shown to be lost in prostate cancer [33].

Once dimerization has occurred, the kinase domain is activated and autophosphorylation of the tyrosine residues within the cytoplasmic tail follows [2]. The signaling cascade is initiated when docking of an adapter protein occurs at the phosphotyrosine residues. Each of the ErbB receptors has a unique pattern of tyrosine residues phosphorylated in the C-terminal tail, specifying which adapter proteins may bind and in turn, which signaling pathways are initiated [32]. ErbB3 comprises six binding sites for the p58 regulatory subunit of the PI3Kprotein (phosphoinositide 3-kinase), enabling direct activation of the PI3K signaling pathway [2, 32]. All members of the ErbB family have binding sites for activators of the MAPK (mitogen activated protein kinase) pathway as well.

Activation of the PI3K pathway involves initial EGFR dimer binding with a PI3K adapter protein, activating downstream AKT which in turn inhibits the FOXO transcription factors, mediators of apoptosis [34]. Activation of the MAPK pathway involves initial binding with a MAPK adapter protein, activating downstream RAS, RAF and MEK which activates downstream MAPK, activating the ELK transcription factor which promotes transcription and cell growth. Gioeli et al measured 82 primary and metastatic prostate tumor samples and showed increasing MAPK activation correlated with increasing Gleason score and tumor stage [35]. These are only two examples of major signaling pathways activated by the EGFR family.

Three main causes of the ErbBs being involved in oncogenesis have been described: 1) increased receptor expression and/or gene amplification, 2) increased ligand expression, and 3) mutations causing constitutive activation of the receptor [2]. Abnormal activity has been linked more to the increased expression of the ligand than mutations in the receptor. ErbB2 overexpression has been associated with metastsis to the bone in both breast and prostate cancer [36]. Overexpression of the ErbB2 and ErbB3 heterodimer has been associated with increased

tumor growth in breast cancer via the PI3K pathway and is thought to promote the metastatic potential of the disease [37]. Chen et al performed a study using prostate cancer samples that were both androgen –dependent and –independent, and concluded that there was a statistically significant increase in ErbB3 expression from androgen –dependent to –independent tumor samples [38]. These findings attest to a significant role for ErbB2 and ErbB3 in prostate tumorgenesis.

Inhibitors of the ErbB protein family have been developed and are now used clinically to treat breast cancer resulting in decreased ErbB2 activity [2]. However, no inhibitor developed against ErbB2 has been effective in clinical trials against prostate cancer. Thus far, inhibitors of ErbB3 have only been mildly considered, since ErbB2 was thought to be the key player in cancer development. Table 1-2 lists ErbB family members with miRNAs proven to target the ErbBs, and cancer in which the interactions have been identified [27]. Knowing that miRNAs function as molecules that either inhibit translation or initiate degredation of their target mRNA, they are interesting as potential biomarkers of the disease or as a possible alternative to drug therapy [39].

Table 1-2: ErbB family members expressed in cancer with proven miRNA interactions.

Protein target	Proven miRNA	Cancer
ErbB1	hsa-miR-7	Lung, Breast, Glioblastoma
ErbB2	hsa-miR-125a	Breast
	hsa-miR-125b	Breast
	hsa-miR-331-3p	Prostate
	hsa-miR-548d-3p	Cervical
	hsa-miR-559	Cervical
ErbB3	hsa-miR-125a	Breast
	hsa-miR-125b	Breast
	hsa-miR-205	Breast

Objectives:

Interest in miRNAs has increased over the last years due to their potential as both biomarkers of disease as well as alternatives to drug therapy. Identification of miRNA targets as well as their contribution to the development of disease has moved to the forefront of cancer research. Traditionally used gene arrays evaluate levels of gene expression and are unable to capture the true nature of protein expression due to post-transcriptional regulation via miRNAs. Furthermore, strictly computational approaches have generated only minor success in identifying crucial miRNA targets due to the many possible conformations of miRNA/target coupling.

Our objective is to take a novel approach. Here, a high throughput proteomics method combined with a computationally derived network is used to identify key proteins driving prostate cancer progression. This approach enables the evaluation of gene expression levels post-transcriptionally in cancer cell lines with key protein node predictions to identify potential miRNA interactions. This analysis coupled with screening of the miRnome (miRNA transcriptome) should enhance the identification of relevant miRNAs dysregulated in prostate cancer which contribute to tumor progression. Additional experiments such as single miR analysis in model prostate cancer cell lines compared to human tumors will further validate the conclusions from this multifaceted approach.

Chapter 2: A Proteomics Approach to identifying Key Proteins dysregulated in Prostate Cancer.

Proteomics and RPMA Technology:

Traditionally, gene arrays have been used to try to predict genes involved in prostate cancer development as well as identify stages of tumor progression [40]. Yet the mechanism behind using gene arrays is to reverse transcribe mRNA into cDNA. Therefore gene expression arrays measure mRNA levels present prior to translation. Since miRNAs regulate levels of gene products driving translation, measuring the actual level of protein products should be a more accurate method of measuring a gene/protein's activity and potential influence in the cell.

Two major types of protein arrays are in use: Forward phase protein microarrays and Reverse Phase Protein Microarrays (RPMA) [41]. Generally, in forward phase protein arrays, the antibody(s) of the protein(s) of interest are spotted on to a glass or silica chip used as a bait molecule, and the chip is incubated with the protein lysate of interest [42]. Using this method, only one type of sample condition can be measured at a time. Conversely, in RPMAs, the cellular lysate is spotted onto the chip in a series of dilutions and the chip is incubated with the antibody to the protein of interest [43]. This miniature dilution curve is designed to insure accurate quantification and to describe the overall dynamic range of protein detection. This method allows for multiple samples to be spotted on the same chip, but requiring one slide for each antibody analyzed. Overall, both methods produce a high-throughput system for measuring expression levels of hundreds of proteins across multiple sample conditions.

Compared to conventional western blotting methods to measure protein expression, protein microarrays are undoubtedly more efficient considering sample size and time consumption [44]. Western blots use on average around 30ug of protein lysate per sample, depending on how abundant the protein of interest is in the specific cell or tissue-type. Protein microarrays can use picograms to femtograms of protein lysate, using only 200 cells total to print one array slide. Anywhere from 5,000 to 20,000 total cells is sufficient to measure protein expression across 100 different proteins of interest.

Tissue Culture Methods:

The 'stock' media used for P69 and M12 cell lines includes: RPMI 1640 media with L-glutamine from Sigma-Aldrich, 5% fetal bovine serum, ITS (5µg/ml insulin 'I', 5µg/ml transferrin 'T' and 5ng/ml selenium 'S') from Collaborative Research in Bedford, MA and 0.05mg/ml gentamycin to prevent bacterial growth contamination. The M12+miR-17-3p cell line contains a stably integrated plasmid and requires puromycin (100µg/µl) in addition to the 'stock' media for selection.

All cell types were grown at 37∘C in 250ml T75 flasks and were split when confluent. Cells were harvested from the flask via scraping over ice and using cold 1xPBS. Cells were pelleted at 1000 rpm in a 15ml conical tube, re-suspended in 1xPBS and pelleted a second time at 5000 rpm in a 1.5ml eppendorf tube. The cell pellets were flash frozen using liquid nitrogen and stored at -80∘C.

For the purpose of this experiment, 1 cell pellet was made from each flask and 3 consecutive passages (denoted as 'T' numbers) of each cell line were harvested. The cell pellets

were then sent on dry ice to Dr. Emanuel Petricoin III's lab at George Mason University's Center for Applied Proteomics and Molecular Medicine.

Reverse Phase Protein Microarray performed at George Mason University:

The cells were lysed prior to spotting in buffer containing 9M urea, 4% 3-[(3-chlamidopropyl) dimethylammonio]-1-propanesulfonate, 2% pH 8.0-10.5 Pharmalyte, and 65mM DTT. Each cell pellet lysate was spotted in a miniature serial dilution curve (neat, 1:2, 1:4, 1:8, 1:16 and buffer) onto a glass nitrocellulose-coated slide. The RPMA protocol as previously described was followed [45]. Overall, antibodies for 111 different proteins were incubated with our various cell lysates to follow protein expression in our prostate cancer progression model. Many of the antibodies were monoclonals' raised against specific phosphorylated residues of the host antigen; thus, used to measure differences in activating various signaling pathways deemed important in cancer. After verification of their internal standards and normalization, the Petricoin lab returned the proteomics results for statistical analysis.

Statistical Analysis of the RPMA data:

Microsoft Excel was used to perform a two-sample equal variance T-Test to compare the protein expression data across the different cell lines provided. A strict probability value (p-value) of $p <= 0.001$ was used to correct for variation among multiple samples and to identify truly significant changes. Those with significant changes were converted into fold changes by dividing the average expression of the protein in one cell line by the average expression of the protein in the comparison cell line. Figure 2-1 depicts the overall process of the statistical analysis using protein ErbB2 as an example.

Figure 2-1: Overview of the Statistical Analysis of the RPMA data.

A T-Test was performed to compare the protein expression data across the different cell lines provided. A p-value of $p \leq 0.001$ was used to correct for multiple samples and to identify truly significant changes. Those with significant changes were converted into fold changes by dividing the average expression of the protein in one cell line by the average expression of the protein in the comparison cell line.

Figure 2-1: Overview of the Statistical Analysis of the RPMA data.

P69 ErbB3	M12 ErbB3
T23- 6173.37	T14- 15630.82
T24- 7186.79	T16- 14647.13
T25- 8192.71	T17- 15382.72

T-Test: 0.0002512199 Significant? p <= 0.001

P69 ErbB3 Avg: 7184.29

M12 ErbB3 Avg: 15220.22

Fold change: P69 -> M12 2X ↑
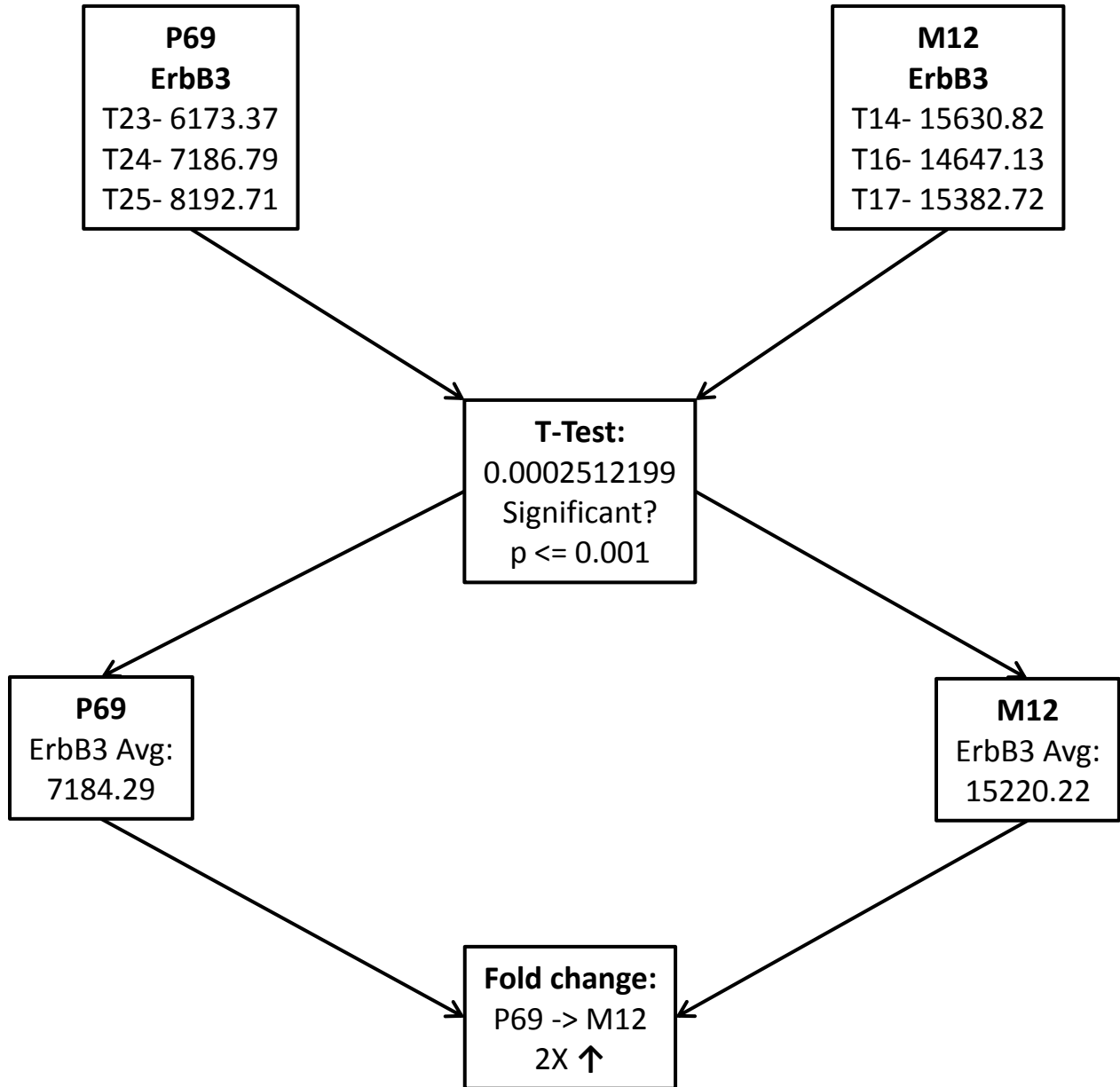
RPMA Findings:

Table 2-1 is an overview of proteins shown to have statistically significant changes in expression level (p-value <= 0.001) within our prostate cancer progression model as measured by RPMA. Phosphorylated c-KIT, ErbB3 and ErbB2 were the most interesting of the proteins changing in our proteomics data, because for the most part they showed significant changes across multiple cell lines. All three proteins showed an increase in expression from the non-tumorigenic P69 cell line to the highly metastatic, tumorigenic M12 subline except there was no significant change (NS) in the phosphorylation status of ErbB2 (phosphorylated Tyrosine 1248). Interestingly, a decrease in expression from the M12 cell line to the weakly tumorigenic, non-metastatic M12+miR-17-3p subline with increased expression of the tumor suppressor miR17-3p was apparent except for ErbB2.

These results are consistent with a protein that is being dysregulated by increased expression in the highly metastatic cell line compared to the non-tumorigenic/poorly tumorigenic variant in our model of disease. Since miR17-3p is dysregulated in the opposite direction in our progression model, (decreasing from P69 to M12 and then increasing from M12 to M12+miR-17-3p), there is a possibility that miR-17-3p may be directly targeting pc-KIT, ErbB3 mRNAs and possibly ErbB2/pErbB2 due to significant changes in at least one direction. Confirmation of direct miRNA/target interactions is imperative in theidentification of possible biomarkers as well as therapeutic options for disease. This hypothesis warrants further testing.

Table 2-1: Fold changes of proteins with statistically significant expression changes based on RPMA.

Protein	P69 → M12 fold change	M12 → M12+miR-17-3p fold change
*pc-KIT	1.7×10^7X ↑	1.7×10^7X ↓
ErbB3	2X ↑	1.3X ↓
ErbB2	1.7X ↑	NS
*pErbB2	NS	1.6X ↓
*pERK	5.1X ↓	NS
*pJak1	NS	1.9X ↓

NS- No significant change
↑ Increase in expression
↓ Decrease in expression
*p = antibody used specific to a phosphorylated residue

Chapter 3: A Networks Approach to Identifying Important miRNA Regulated Proteins in Prostate Cancer

Networks Biology:

The human body, organs, cells are all very complex systems that require intricate coordination and proper execution of a remarkable number of biological processes in order to perform properly [46]. Thus far, 5 main types of biological networks have been characterized to help better understand these biological processes and to observe how the smaller pieces create the whole. These networks include transcription factor-binding, phosphorylation, metabolic, genetic, and protein-protein interaction. Focusing on protein-protein interaction networks, the proteins are considered nodes, and interactions between the nodes are represented as edges. The interaction of proteins with other proteins in the cell plays a key role in most biological processes [47]. The evaluation and identification of all protein-protein interactions within the cell is thought to be the key to uncovering how cells function on a large-scale, under normal and disease conditions.
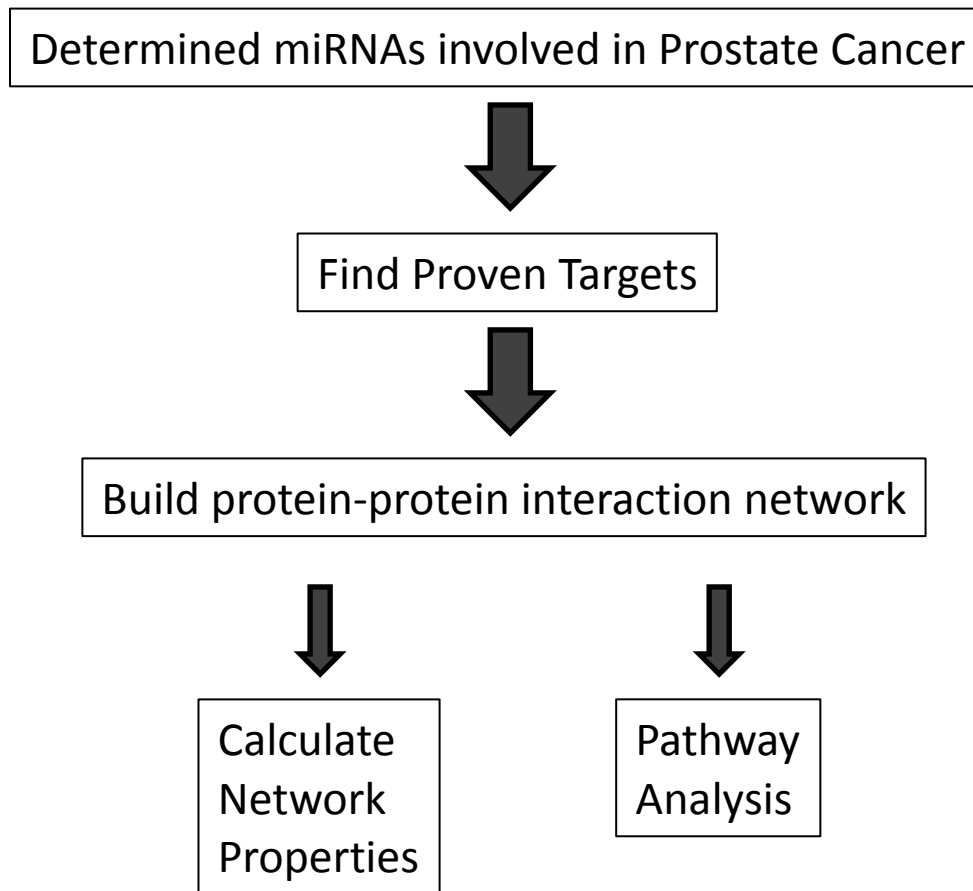
Building a protein-protein interation network of proven targets of miRNAs shown to be dysregulated in the Prostate:

Figure 3-1 depicts the process of building the protein-protein interaction network of proven targets of miRNAs dysregulated in the prostate. A list of 111 dysregulated miRNAs, associated with the development of prostate cancer was obtained from the miR2Disease online resource [48]. The database was interrogated using the included html search function using the query term "prostate carcinoma". Causal and unspecified relationships were included. A PERL script was written to extract each miRNAs expression pattern and literature reference.

Figure 3-1: Overview of building a protein-protein interaction network of proven targets of miRNAs dysregulated in the prostate.

miRNAs dysregulated in the prostate were obtained from the miR2Disease database [48].

Experimentally proven miRNA/target interactions were obtained from joining the information in

the Tarbase and miRecords repositories [27, 49]. Prostate transcriptome profiles were obtained from

Unigene to determine transcripts expressed in the prostate [50]. Agilent and Cytoscape were used in

conjunction to build the protein-protein interaction networks. The network properties were

calculated using CentiScaPe [51-53].

Figure 3-1: Overview of building a protein-protein interaction network of proven targets of miRNAs dysregulated in the prostate.

Determined miRNAs involved in Prostate Cancer

↓

Find Proven Targets

↓

Build protein-protein interaction network

↓   ↓

Calculate Network Properties   Pathway Analysis

A table of all known miRNA/gene interactions was assembled by combining the information in Tarbase and miRecords, repositories of experimentally supported miRNA target interactions that were downloaded in May of 2011[27, 49]. A PERL script was written to compile the data extracted from both repositories to create a single non-redundant list. Using the miR2Disease list of miRNAs dysregulated in the prostate, a comprehensive list of validated targets associated with these miRNAs was created [48].

Transcriptome profiles for the prostate gland were obtained from the Unigene database [50]. A prostate specific protein-protein interaction network was built. A PERL script was used to extract identifiers of transcripts that showed any level of expression in the prostate gland, the identifiers were then converted to HUGO gene symbols. There were a total of 608 confirmed proteins identified that are reported targets of miRNAs dysregulated in the prostate. These were obtained by combining the comprehensive list of validated miRNA/target interactions and the list of transcripts expressed in the prostate.

Using Cytoscape 2.8 along with the Agilent literature search (v2.76) tool, two literature mined prostate protein-protein interaction networks were inferred [51, 52]. For the first network, each protein in the list of 608 known prostate cancer miRNA target proteins was used as a search term in the Agilent literature search tool and the search was controlled to limited interactions to Homo sapiens with a maximum of 10 hits per search string/search engine. The second, random network, was built in the same manner using 608 randomly chosen proteins expressed in the prostate gland according to the Unigene database, disregarding known miRNA status[50]. Visualization was accomplished using Cytoscape and topological network descriptors were estimated using CentiScaPe [53].

The random network built was shuffled 50,000 times using a degree preserving edge shuffle random network plugin developed by engineers at Syracuse University and implemented in Cytoscape. The plugin was downloaded (http://sites.google.com/site/randomnetworkplugin/Home) as a .jar file and installed in the Cytoscape package.

Statistical analysis of the Networks:

Differences in network distributions were evaluated using an Analysis of Variance test (ANOVA) with significance set at probability ≤ 0.05. All statistical analyses were performed using JMP 8.0 (Statistical Analysis Software Cary, NC). The distribution of node degree for the prostate miRNA targeted network and the random network were created using the R Project for Statistical Computing (http://www.r-project.org/).

Network Findings:

In networks analysis, node degree can be used to surmise the proteins contribution to the stability of the network/cell. Node degree represents the maximum interaction potential of a protein. A random protein-protein interaction network of proteins was compared to the results obtained from the miRNA/proven target network and determine the likelihood that the interaction would have been seen due to chance alone. Table 3-1 shows the node degree distribution differences between the random network of proteins expressed in the prostate compared to the miRNA/proven target network of proteins [54]. The analysis shows that there is an enrichment of more highly connected nodes in the miRNA/proven target network than the network of randomly chosen proteins expressed in the prostate. The random network had an average node degree of 5 opposed to the miRNA/target networks average node degree of 30.

Table 3-1: A comparison of node distributions between the random network of proteins expressed in the prostate and the miRNA/proven target Prostate Cancer network.

Network	Mean Node Degree	Standard Deviation	Minimum	Maximum
Prostate Cancer miRNA target protein	29.80	47.47	1	290
Random prostate protein	4.46	4.24	1	28

The high average node degree implies that miRNAs preferentially target transcripts that impact a large number of proteins in the cell. The miRNA/proven target network had a maximum node degree of 290 compared to the random network which had a maximum node degree of 28. It has been shown that molecules with higher node degrees are more essential to cell growth and function [55]. Perturbations of such highly connected nodes have an increased likelihood of negatively impacting the stability of the network/cell [46], leading to a variety of diseases such as cancer [56].

The 608 proteins proven to interact with miRNAs dysregulated in the prostate were ranked based on their node degree. ERBB2 and ERBB3, both members of the epidermal growth factor receptor (EGFR) family, were found to be differentially expressed at a statistically significant level across P69, M12, and M12+miR17-3p cell lines in our proteomics analysis. Table 3-2 depicts the results of the EGFR protein family represented in the protein-protein interaction network of proven target/miRNA interactions [54]. The EGFR family was found to be the 6th highest ranked node in our miRNA target network. The higher node degree infers the importance of this protein family to the stability of the cell/network.

Perturbation of the EGFR family within the cell, potentially by a miRNA, could prove detrimental to the stability and health of the cell. ErbB2 and ErbB3 show a significant increase in expression between the non-tumorigenic P69 cell line and the highly tumorigenic, highly metastatic M12 subline, as well as a high node degree of 248 in our miRNA/target network. From these results, we believe that ErbB2 and ErbB3 have the potential to play a key role in the development of prostate cancer. However, the identification of the cause and consequences of the dysregulation of ErbB2 and ErbB3 is necessary to ultimately prove their role in disease.

Table 3-2: Protein node connectivity results for EGFR.

Protein	Node Degree	Function	Known miRNAs
EGFR	248	Cell proliferation	hsa-miR-7, hsa-miR-125b, hsa-miR-125a, hsa-miR-331-3p, hsa-miR-548d-3p, miR-hsa-559, hsa-miR-205

Chapter 4: Identification of possible miRNA/ErbB2 or ErbB3 interactions.

Screening of the miRnome:

qRT-PCR based microarrays have been developed to produce a high-throughput method of screening miRNA expression levels of all currently known miRNAs in order to identify key players in different diseases. Exiqon has developed the miRCURY LNA microRNA Arrays (catalog # 203607, miRNA human panel 1 and 2 V2.M) for screening of the miRnome (microRNA transcriptome) using two 384 well plates. Total RNA was extracted using the miRVana miRNA Isolation Kit from Invitrogen and 50ng of RNA from each cell type was converted to cDNA using the Exiqon miRCURY LNA Universal RT miRNA PCR kit. The ABI 7900-HT Fast Real-Time PCR System from Applied Biosystems (ABI) was used to amplify and quantify the expression of 700 known miRNAs using recommended settings (95◦ C for 10 minutes, followed by 40 cycles of 95◦ for 10 seconds and 60◦C for 1 minute).

Utilizing GenEx software from Exiqon, Interplate calibration was performed to minimize interplate variation. The cycle threshold (CT) for each microRNA was then normalized to the global mean of the array plate (CT- mean CT). Undetectable expression levels were set greater than the highest normalized CT value observed for that particular cell line. The P69 cell line normalized expression value was used as the calibrator. Table 4-1 shows the miRNA that was the most differentially expressed in our prostate cancer progression model. Achieving a fold change of this magnitude is possible when the expression level of miR125b is very high in one cell line (P69) and very low in the comparison cell line (M12). miR125b was proven to target ERBB2 and ERBB3 in breast cancer and CASP6, CASP7 and BAK1 in prostate cancer. Single miR

Table 4-1: Results of the most differentially expressed miRNA in our miR screen.

miRNA	P69 → M12	Proven Targets	Cancer
miR125b	9055X ↓	ERBB2, ERBB3 CASP7, CASP6,BAK1 (50+ total)	Breast Prostate

analysis is required to confirm the significance of miR125b dysregulation in our prostate progression model.

Single miR analysis of miR125b:

Single miR analysis of miR125b expression in our prostate cancer progression model was performed to verify the results of the Exiqon miR screen. Total RNA was extracted as previously described in the above section. The TaqMan microRNA Assay Kit (Kit # 000449) from ABI was used to convert 20ng of RNA from P69 and M12 cells to cDNA, and subsequently analyzed in triplicate by qRT-PCR. TaqMan probes of RNU48 and miR125b were used in the qRT-PCR reaction using the ABI 7300 Real-Time PCR system with recommended settings (95∘ C for 10 minutes, followed by 40 cycles of 98∘ for 15 seconds and 60∘C for 1 minute). Expression mean values were normalized to RNU48 and the P69 cell line was used as the calibrator. Figure 4-1 depicts the relative level of miR125b expression in the M12 cell line compared to the P69 cell line. A 19.7-fold decrease in miR125b expression was observed from the P69 cell line to the M12 cell line.

To verify the dysregulation of miR125b in human prostate tissue, single miR analysis of miR125b expression in benign, stroma, prostatic intraepithelial neoplasia (PIN), benign prostatic hyperplasia (BPH) and tumor cells was performed. The patient sample was obtained from the Virginia Commonwealth University Anatomic Pathology Tissue Depository with approved IRB protocol. The protocol for laser-capture microdissection (LCM) of formalin-fixed paraffin-embedded (FFPE) patient samples was followed as previously described by Zhang et al [31]. Total RNA was extracted from benign, stroma, PIN, BPH and tumor tissue using the PicoPure RNA extraction kit from Life Technologies. RNA quantity and integrity were assessed using the

41

Figure 4-1: The relative level of miR125b expression in the M12 cell line compared to P69.

Total RNA was extracted from M12 and P69 cell pellets, 20ng of each RNA extract was

converted to cDNA and qRT-PCR was performed (in triplicate). Expression level means were

normalized to RNU48 and the P69 normalized value was used as the calibrator. Standard

deviation within each sample is shown.

Figure 4-1: The relative level of miR125b expression in the M12 cell line compared to P69.
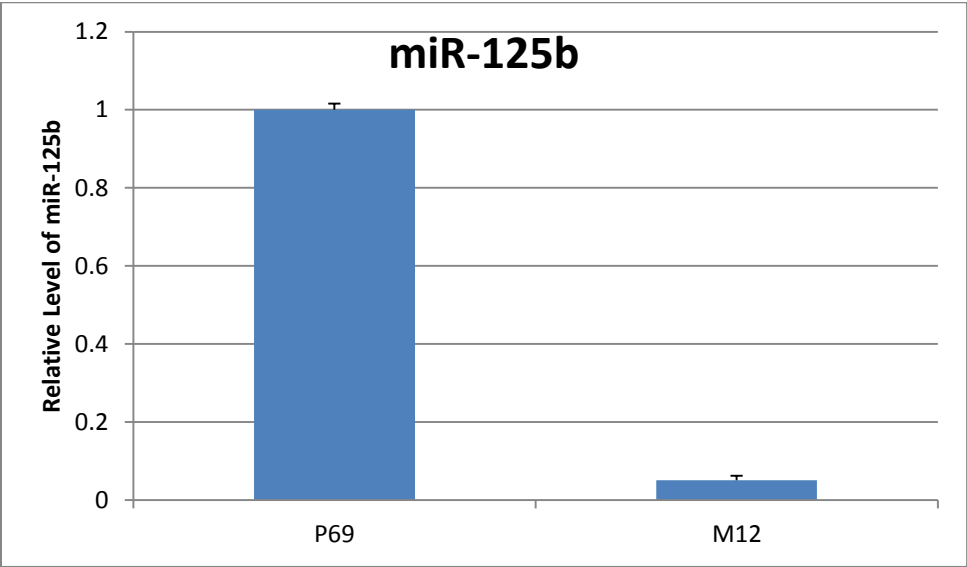
Agilent Bioanalyzer. cDNA conversion and qRT-PCR was performed in triplicate using the TaqMan assay as previously described. The mean expression values of each sample were normalized to RNU48 and the benign normalized expression value was used to calibrate all samples.

Figure 4-2 depicts the relative level of miR125b expression in stroma, PIN, BPH and tumor tissue compared to benign tissue expression. A 1-fold increase in miR125b expression was observed from benign to stroma tissue. A 2.75-fold decrease in expression was observed from benign to PIN tissue with a 2.82-fold decrease from benign to BPH tissue. A substantial 2452-fold decrease in expression was observed from benign to tumor tissue.

Although only one individual human sample was tested, the result of the single miR analysis of miR125b expression in human tissue was consistent with the single miR data and miR screen analysis of our prostate cancer progression model. miR125b expression was significantly lower in the highly metastatic, highly tumorigenic M12 cell line within both the miR screen and individual miR analysis compared to the non-tumorigenic P69 cell line. Also, miR125b expression was significantly lower in human tumor tissue compared to benign tissue.

Figure 4-2: The relative level of miR125b expression in stroma, PIN, BPH and tumor tissue compared to benign tissue of one individual human prostate sample.

LCM of FFPE tissue was performed. Total RNA was extracted and was converted to cDNA.

qRT-PCR was performed and the expression means were normalized to RNU48. Expression

values of all tissues were calibrated to normalized benign tissue expression. Standard deviation

within each sample is shown.

Figure 4-2: The relative level of miR125b expression in stroma, PIN, BPH and tumor tissue compared to benign tissue of one individual human prostate sample.
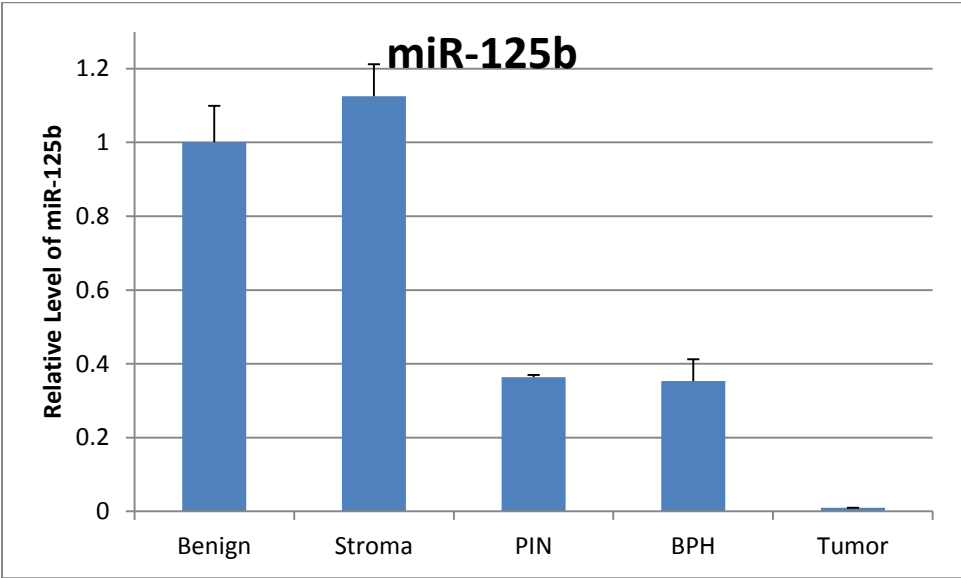
The potential for miR125 to target ErbB2 or ErbB3:

Our computational networks approach to identify key proteins that are influenced by miRNAs dysregulated in prostate cancer suggested the ErbB family of proteins. These proteins are highly connected nodes in the prostate cancer network suggesting that they are key players in the development/progression of prostate cancer. Additionally, our proteomics analysis of the prostate cancer progression model showed that ErbB2 and ErbB3 are significantly dysregulated between P69 -> M12.Overall the results from analyzing the miRnome of our prostate cancer progression model, verified by single miRNA analysis, identified miR125b as being the most differentially expressed tumor suppressing miRNA in our cell lines. Scott et al proposed that miR-125b binds directly to position 19-44 within the 3' UTR of ErbB2 (5'-GCAGAAGCCCUGAUGUGUCCUCAGGGA-3') and position 8-26 of ErbB3 (5'-UCCCUGUGGCACUCAGGGA-3') controlling metastatic potential of breast cancer cells [20]. Based on the reported results, it is reasonable to postulate that miR125b could be directly targeting ErbB2 and ErbB3 in prostate cancer via the binding sites described above.

Computational analysis of ErbB2 and ErbB3 3'UTRs and miR125b:

The 3'UTR sequences for ErbB2 and ErbB3 were obtained from the National Center for Biotechnology Information (NCBI) and the sequence for miR125b was obtained from miRBase [27, 57, 58]. The miR125b sequence and 3'UTR sequences of ErbB2 and ErbB3 were submitted to RNAhybrid, a miRNA/RNA minimum free energy structural hybridization prediction tool, using the default settings [59]. Figure 4-1 depicts the predicted structural interaction of miR125b and the 3'UTRs of ErbB2/ErbB3. Many of the proven miRNA binding sites have perfect seed region (bases 2-8) Watson-Crick binding, adequate minimum free energy of formation (deltaG < -20.0

Figure 4-1: Previously described miR125b coupling with the 3'UTR of ErbB2 or ErbB3.

The sequences of the complete 3'UTR of (A) ErbB2/ (B) ErbB3 and the sequence of miR-125b were compared using RNAhybrid to predict potential interactions of miR-125b (green) with the 3' UTRs of ErbB2/ ErbB3 (red) [59]. Potential structures and the minimum free energy of formation of the binding sites proposed by Scott et al are shown.

Figure 4-1: Previously described miR125b coupling with the ErbB2 or ErbB3 3'UTRs.
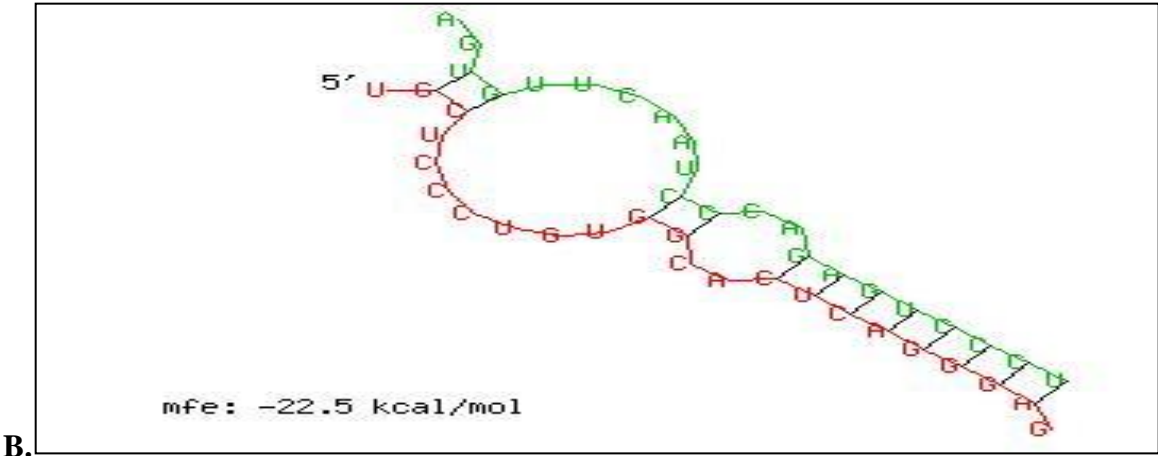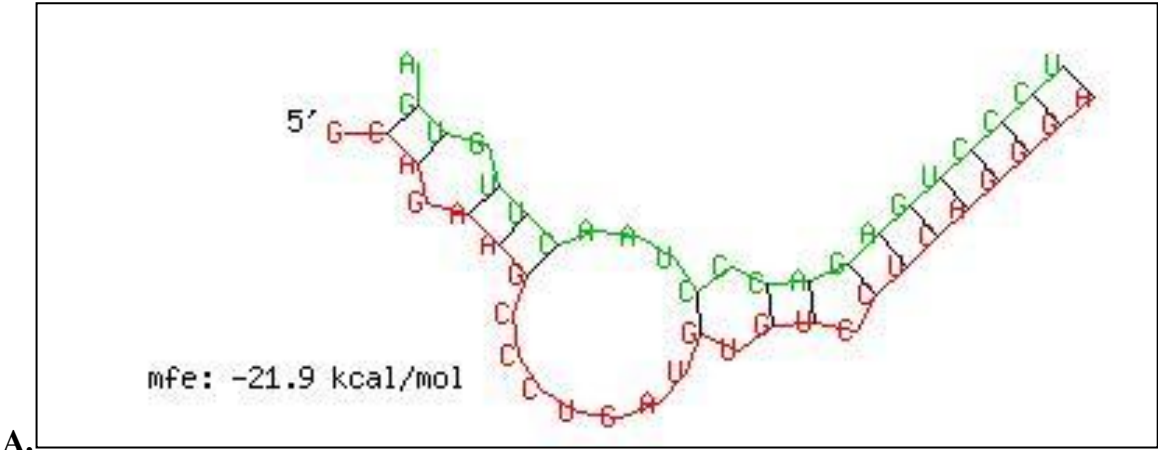
kcal/mol), and some degree of 3' stabilization. The structure of the proposed binding sites for both proposed miRNAs adhere to previously observed characteristics and thus it is reasonable to suspect that these interactions would occur *in vivo*.

Mutation of seed region binding in the 3'UTRs of ErbB2 and ErbB3 is required to determine if these are true miRNA/target interactions within the prostate gland and if these interactions may be contributing to the development of prostate cancer. In order to evaluate potential binding, a reporter construct containing mutations of three bases (2-4, GGG to TTT) within the 3'UTRregion of ErbB2 and ErbB3 proposed to be under miR-125b regulation was constructed. To confirm that the mutations decrease the likelihood of microRNA regulation, the mutated sequence was evaluated using RNAhybrid. Since complete seed region binding does not exist, there is a poor minimum free energy. Most likely neither the mutant ErbB2 3'UTR or the mutant ErbB3 3'UTR are likely to be under the control of miR-125b regulation (Figure 4-2).

Figure 4-2: miR125b coupling with the mutated ErbB2 and ErbB3 3'UTRs.

The sequences of the proposed mutant 3' UTR of (A)ErbB2 / (B)ErbB3 and the sequence of

miR-125b were compared using RNAhybrid to predict potential interactions of miR-125b

(green) [59]. Potential structures and the minimum free energy of formation of the mutant binding

sites are shown.

Figure 4-2: miR125b coupling with the mutated ErbB2 and ErbB3 3'UTRs.

A.

B.
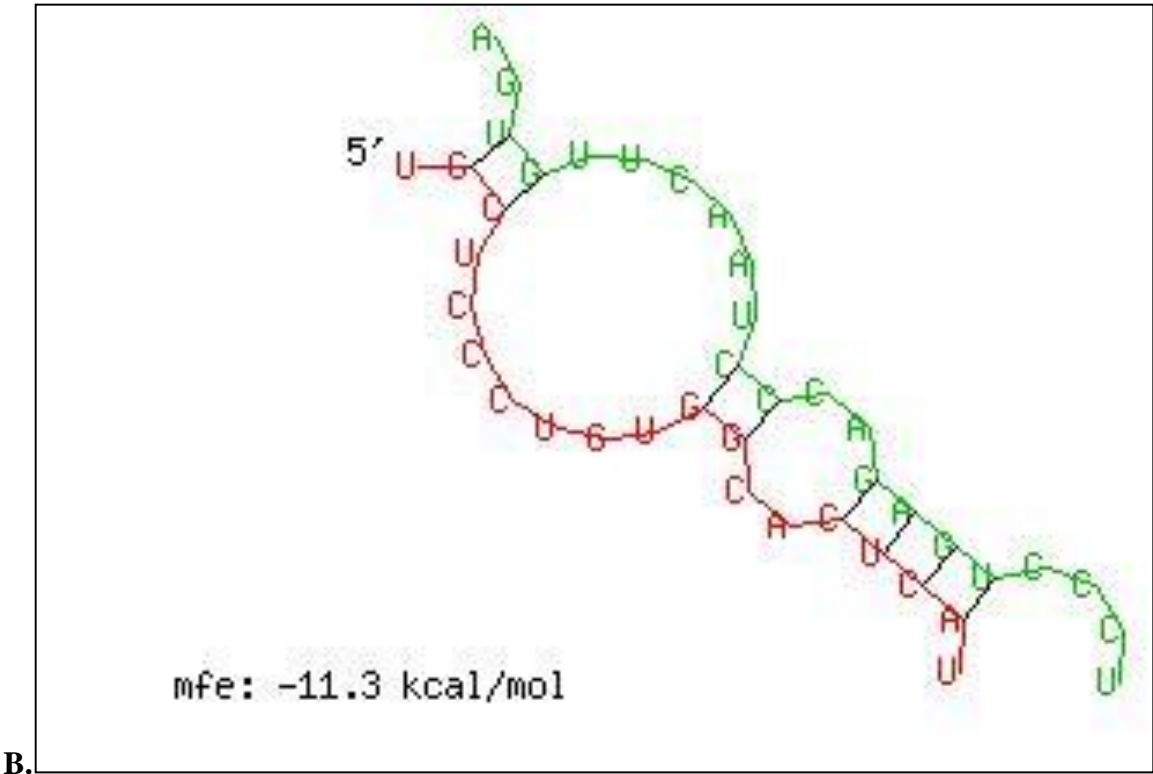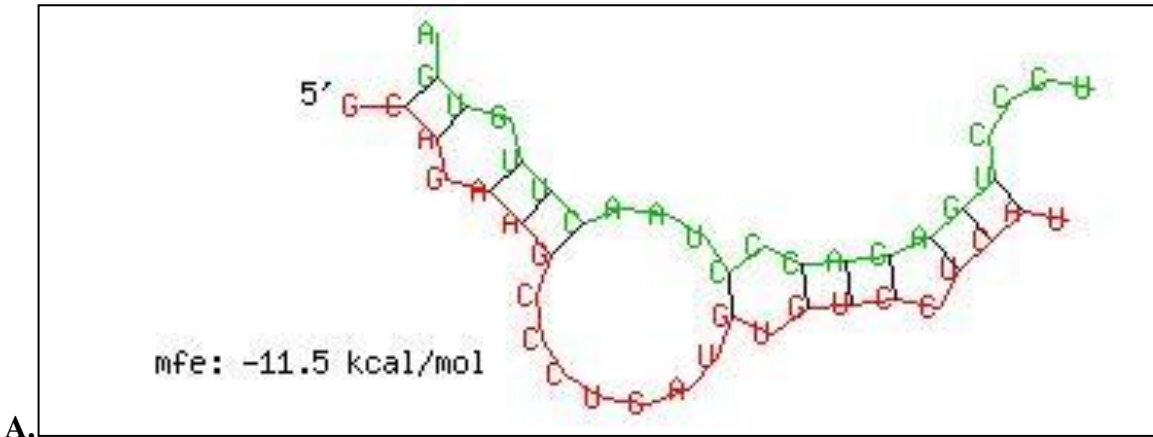
ErbB2 and ErbB3 oligonucleotides:

Eight custom oligonucleotides were synthesized (Invitrogen), including both forward and reverse strands of the wild type (wt) and mutant (mut) ErbB2 as well as ErbB3 3'UTR segments. Each annealed oligonucleotide pair on the 5'-end was synthesized with a blunt DraI restriction enzyme recognition sequence followed by an internal full NotI restriction enzyme recognition sequence, the requisite ErbB2 or ErbB3 3'UTR sequence and a 3'-end sticky XbaI restriction enzyme recognition sequence for proper insertion into the multiple cloning site (digested with DraI/XbaI) of the pmiRGlo vector (Promega). Figure 4-3 displays the ErbB2 and ErbB3 wt and mut oligonucleotides synthesized for insertion into the pmiRGlo vector (Promega). A three base pair mutation within the miR125b seed binding region (bases 2-4) was achieved by changing GGG to TTT.

The lyophilized oligos were re-suspended in TE buffer to a final concentration of 200uM and stored at -20◦C. Oligonucleotides were annealed in a 20ul reaction containing 5ul each of a forward and reverse strand, 2ul of 10X Oligo annealing buffer (100mM Tris-HCL, 10mM EDTA, 1M NaCl) and 8ul of DNAse/RNAse free water. Annealing was accomplished by incubation at 95◦C for 4 minutes on a heat block, followed by gradual cooling at room temperature for one hour. Annealed oligos were stored at -20◦C.

Figure 4-3: ErbB2 and ErbB3 wild type and mutant synthesized oligonucleotides:

Each annealed oligonucleotide pair on the 5'-end was synthesized with a blunt DraI restriction enzyme recognition sequence followed by an internal full NotI restriction enzyme recognition sequence, the requisite ErbB2 or ErbB3 3'UTR sequence and a 3'-end sticky XbaI restriction enzyme recognition sequence for proper insertion into the multiple cloning site (digested with DraI/XbaI) of the pmiRGlo vector (Promega). A three base pair mutation within the miR125b seed binding region (bases 2-4) was achieved by changing GGG to TTT.

Figure 4-3: ErbB2 and ErbB3 wild type and mutant synthesized oligonucleotides:

```
ErbB2wt:
5'- AAACTAGCGGCCGCAGGCCAAGTCCGCAGAAGCCCTGATGTGTCCTCAGGGAGCAGGGAAGGT        -3'
3'- TTTGATCGCCGGCGTCCGGTTCAGGCGTCTTCGGGACTACACAGCAGTCCCTCGTCCCTTCCAGATC -5'
```

```
ErbB2mut:
5'- AAACTAGCGGCCGCAGGCCAAGTCCGCAGAAGCCCTGATGTGTCCTCATTTTAGCAGGGAAGGT        -3'
3'- TTTGATCGCCGGCGTCCGGTTCAGGCGTCTTCGGGACTACACAGCAGTAAATCGTCCCTTCCAGATC -5'
```

```
ErbB3wt:
5'- AAACTAGCGGCCGCCTCCTGCTCCCTGTGGCACTCAGGGATTAGGGAATGGATAAGAGTGCCT        -3'
3'- TTTGATCGCCGGCGGAGGACGAGGGACACCGTGAGTCCCTAATCCCTTACCTATTCTCACGGAGATC -5'
```

```
ErbB3mut:
5'- AAACTAGCGGCCGCCTCCTGCTCCCTGTGGCACTCATTTATTAGGGAATGGATAAGAGTGCCT        -3'
3'- TTTGATCGCCGGCGGAGGACGAGGGACACCGTGAGTAAATAATCCCTTACCTATTCTCACGGAGATC -5'
```

DraI-Restriction site
NotI-Blunt end
XbaI-Sticky end
miR125b target site
miR125b target mutation

ErbB2 and ErbB3 plasmid cloning:

The pmiRGlo vector (2µg) was digested with 2-units of DraI (New England Biolabs - NEB), 2 units of XbaI (NEB) in NEB buffer 4 with 1xBovine Serum Albumin ('BSA' from NEB) and brought up to a 20µl reaction volume with DNAse/RNAse free water. The sample was incubated in a water bath at 37∘C for 1 hour and 30 minutes. Heat inactivation of the enzymes was achieved by heating the sample for 20 minutes on a heat block at 65∘C. The ligation reaction was set up so that there was an 8:1 insert (400ng) to vector (50ng) ratio. In a reaction volume of 20µl, the mixture contained 1xT4 DNA Ligase buffer (NEB) and 2-units of T4 DNA ligase (NEB). The sample was incubated at 25∘C for 1 hour.

Competent DH5-alpha *E.* coli cells (50 µl) were transformed with the ligation mixture (10 µl). Transformation was accomplished by incubation on ice for 30 minutes, followed by a 45 second heat-shock at 42∘C and then 2 minutes on ice. Pre-warmed (37∘C) Luria Broth (LB) media (950µl) was added to each mixture and incubated for 1 hour (37∘C with 225 rpm). Colony selection was accomplished by plating 200ul and 50ul of each transformation onto LB+Ampicillin (0.1µg/ml) plates and incubated overnight at 37∘C. Single colonies from each transformation were selected and used to inoculate 250ml of LB+Ampicillin media (0.1µg/ml) per sample and incubated overnight (37∘C with 225 rpm). Maxipreps of the inoculates were performed using the PowerPrep Plasmid Purification Kit from Origene with integrated pre-filters following the manufacturer's protocol. The DNA sequence of the various 3'UTR inserts was verified by the Nucleic Acids Research Facilities (NARF) at Virginia Commonwealth University.

Cell line Transfections with ErbB2 and ErbB3 wild type and mutated 3'UTRs:

P69 and M12+miR17-3p cell lines were transfected with the entire 3'UTR of ErbB2 and ErbB3 inserted into the XbaI restriction site of the PGL3 promoter vector (PGL3 vector +3'UTR of pErbB2 or pErbB3) fused 3'- to the firefly luciferase gene. The constructs were provided to us by Dr. Christopher C. Benz at the Buck Institute for Age Research, Novato, CA [20]. In addition, the P69 cell line was transfected either with the wild type or mutated 3'UTR constructs of ErbB2 and ErbB3 inserted into the pmiRGlo vector as previously described. Prior to transfection, 200,000 actively growing cells were plated per well in triplicate on a 6 well plate and cultured at 37◦C for 24 hours. Cells were cultured and passed at least twice before transfection and counted using a Beckman-Coulter particle counter.

Transfection was accomplished with TransIT transfection reagent from Mirus (2µg TransIT/ng DNA) and incubated at room temperature for 5 minutes with serum free RPMI 1640 media plus L-glutamine (Sigma-Aldrich). For the PGL3 constructs, purified plasmid (1µg) either PGL3 vector with no insert or PGL3 vector plus pErbB2 or pErbB3 3'UTRs was complexed with transfection reagent plus the renilla luciferase control reporter vector (15ng). The optimal ratios of PGL3 and renilla plasmid were previously determined[31]. For the pmiRGlo constructs, purified plasmid (250ng) was complexed with transfection reagent creating these test samples, pmiRGlo with no insert or pmiRGlo with pErbB2wt, pErbB2mut, pErbB3wt or pErbB3mut 3'UTRs. Each sample was incubated for 30 minutes at room temperature. Fresh media as previously described for each cell type was added to each well and the TransIT/RPMI/plasmid mixture was dripped over each well shaking gently side to side. The amount of DNA utilized for the pmiRGlo vector and incubation time were determined empirically and found to produce the most favorable results.

After 48 hours of incubation at 37∘C, the cells were lysed for 30 minutes directly on the plate with passive lysis buffer (Promega). Cell lysates were stored at -80∘C for ~24 hours. Reporter activity was measured using the Promega Dual Luceriferase Assay Kit. Cell lysates and reagents were warmed to room temperature per manufacturer's instructions. Reporter activity (firefly luciferase) was quantified using 30µl of the cell lysate plus 30µl of the luciferase assay reagent II (LAR II) and measured with a Glowmax Luminometer. Control reporter activity (Renilla luciferase) was assayed in the same manner after the addition of 30µl of the Stop & Glow reagent. Reporter activity is presented as a ratio of firefly luciferase to renilla luciferase activity.

**Findings of the ErbB2 and ErbB3 Transfections in P69 cells:**

The P69 cell lines were first transfected with the PGL3 plasmids containing the entire ErbB2 or ErbB3 3'UTR sequence to determine if an actual affect was detected within our prostate cancer progression model (Figure 4-4). The non-metastatic P69 cell line was chosen since this cell type exhibits a higher level of miR17-3p expression compared to the M12 cell line. A 2.8-fold or 2.4-fold decrease in expression was observed when comparing the mean expression of the PGL3 empty vector to the mean expression of the pErbB2 or pErbB3 3'UTR containing vectors respectively. Based on these results, translation of both the ErbB2 and ErbB3 mRNAs are being influenced by some non-coding RNA molecule that is binding within the respective 3'UTRs.

The P69 cell line was also transfected with the pmiRGlo vector containing ErbB2wt, ErbB3mut, ErbB3wt and ErbB3mut 3'UTR sequence to determine if miR125b is directly targeting ErbB2 or ErbB3 mRNAs within our prostate cancer progression model. Figure 4-5

Figure 4-4: The 3'UTRs of pErbB2 and pErbB3 repress luciferase reporter activity.

P69 cells (200,000 cells per well) were transfected in triplicate with 1µg of PGL3 empty vector, or vector containing the entire pErbB2 or pErbB3 3'UTR sequences. Luciferase activity was measured 48 hrs later and expressed as the ratio of firefly to renilla. Standard deviation within each sample is shown.

Figure 4-4: The 3'UTRs of pErbB2 and pErbB3 repress luciferase reporter activity.
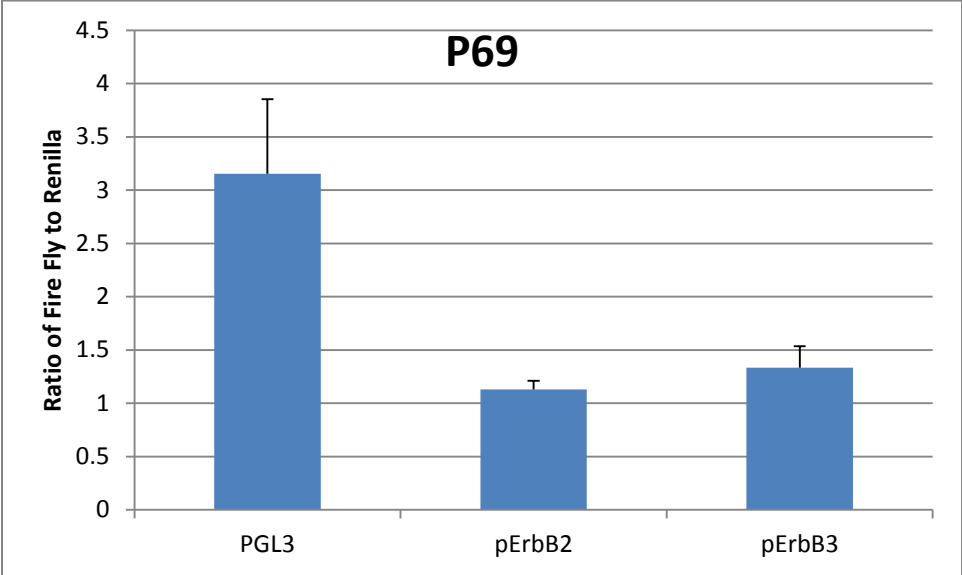
Figure 4-5: miR125b does not directly affect luciferase expression of ErbB2 and ErbB3 wt and mut vectors in the P69 cell line.

P69 cells (200,000 cells per well) were transfected in triplicate with 250ng of pmiRGlo empty

vector, pErbB2wt, pErbB2mut, pErbB3wt or pErbB3mut plasmids. Luciferase activity was

measured 48 hrs later and expressed as the ratio of firefly to renilla. Standard deviation within
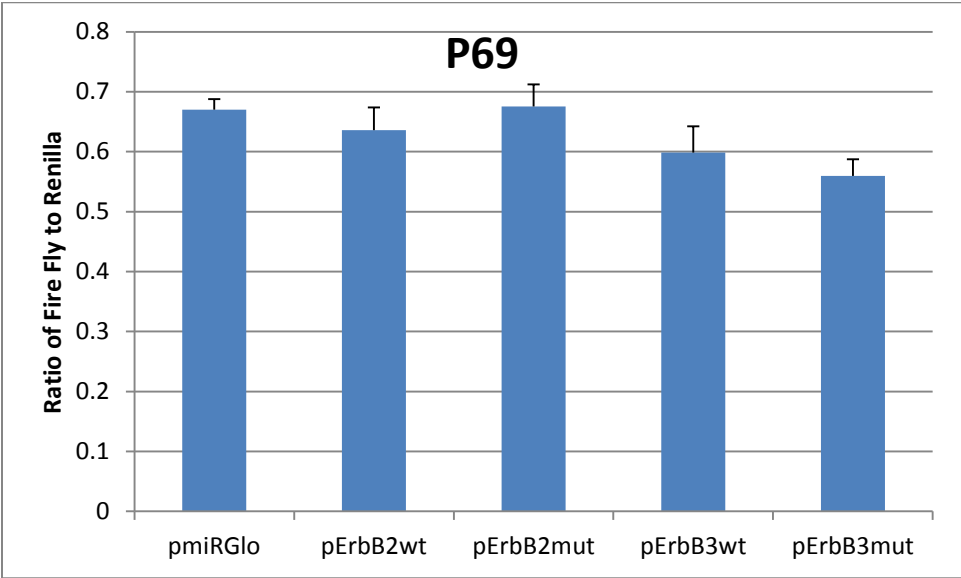
each sample is shown.

Figure 4-5: miR125b does not directly affect luciferase expression of ErbB2 and ErbB3 wt and mut vectors in the P69 cell line.

depicts the results from the transfections of pmiRGlo, pErbB2wt, pErbB2mut, pErbB3wt and

pErbB3mut in the P69 cell line. The P69 cell line was chosen because it has the highest

endogenous expression of miR125b in our prostate cancer progression model. If there was a

direct interaction between miR125b and the ErbB2 and ErbB3 3'UTRs we would have expected

a decrease in luciferase expression between pmiRGlo and the pErbB2wt or pErbB3wt. Based on

these results, no direct binding within the 3'UTRs of ErbB2 and ErbB3 at the miR125b proposed

binding sites identified by Scott et al could be detected by this assay method [20].

The potential for miR17-3p to target ErbB2 or ErbB3:

In addition to our computational networks identification of the ErbB family of proteins as

key players in the development/progression of prostate cancer, our proteomics analysis of the

prostate cancer progression model showed that ErbB2 and ErbB3 are significantly dysregulated

between M12→M12+miR-17-3p. Based on these results, we propose miR17-3p may directly

bind to the 3'UTRs of either or both ErbB2 and ErbB3, which would identify a new

miRNA/target interaction.

Computational analysis of ErbB2 and ErbB3 3'UTRs and miR17-3p:

The sequence for miR17-3p was obtained from miRBase [57, 58].The miR17-3p sequence

and 3'UTR sequences of ErbB2 and ErbB3 were submitted to RNAhybrid, a miRNA/RNA

minimum free energy structural hybridization prediction tool, using the default settings [59]. Figure

4-6 depicts the predicted structural interaction of miR17-3p and the 3' UTRs of ErbB2/ErbB3.

Many of the proven miRNA binding sites have near perfect seed region (bases 2-8) Watson-

Crick binding, adequate minimum free energy of formation (deltaG < -20.0 kcal/mol), and some

Figure 4-6: Predicted miR17-3p coupling with the 3'UTR of ErbB2 or ErbB3.

The sequences of the complete 3' UTR of (A) ErbB2 /(B) ErbB3 and the sequence of miR17-3p were compared using RNAhybrid to predict potential interactions of miR17-3p (green) with the 3' UTRs of ErbB2/ ErbB3 (red) [59].

Figure 4-6: Predicted miR17-3p coupling with the ErbB2 or ErbB3 3'UTRs.
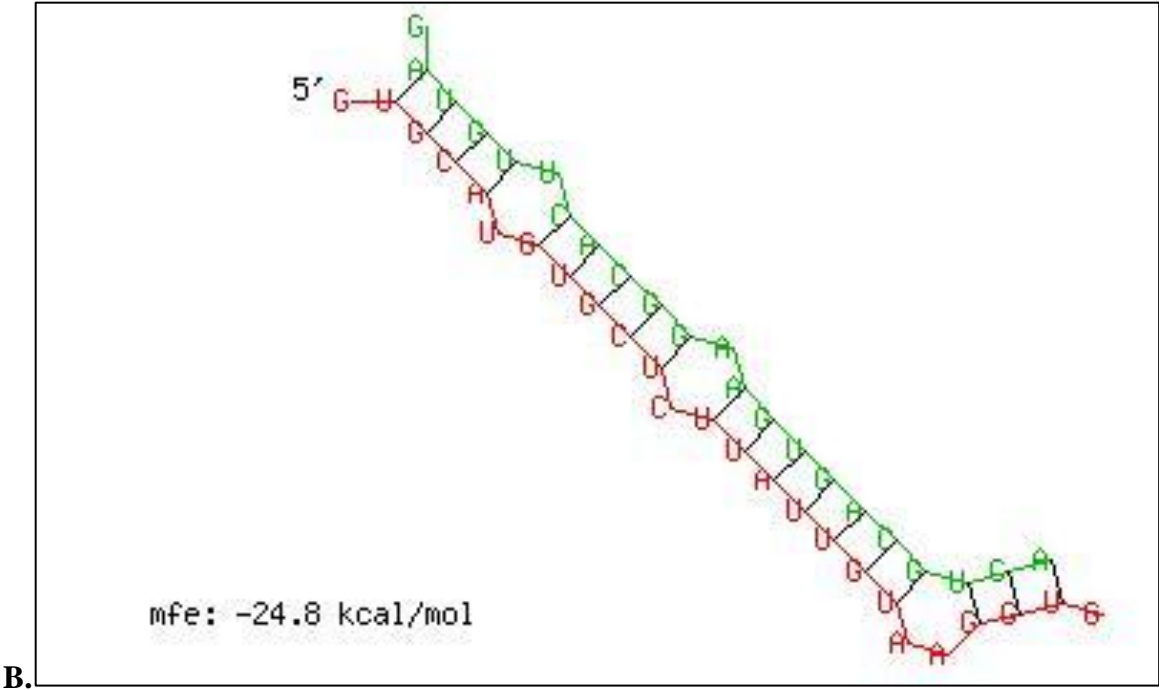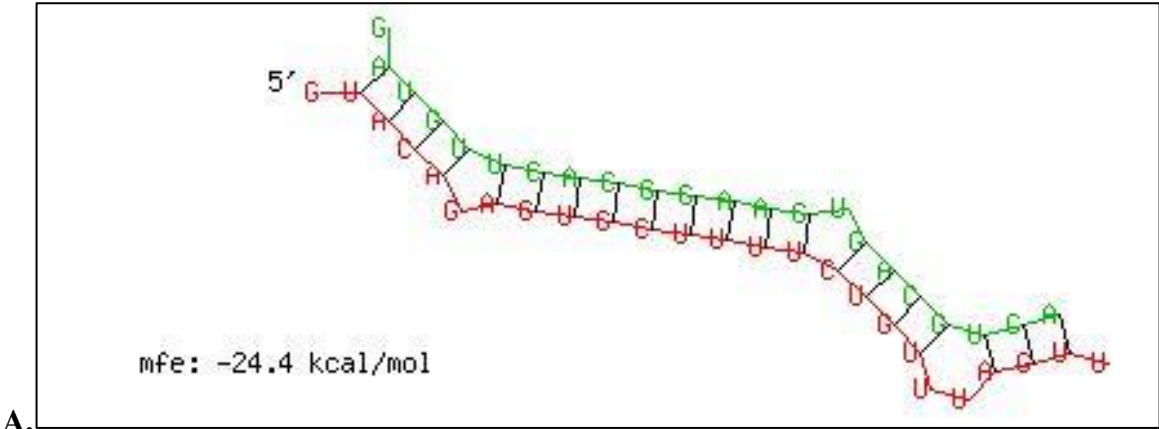
mfe: -24.4 kcal/mol

A.

mfe: -24.8 kcal/mol

B.

degree of 3' stabilization. The structure of the proposed binding sites for both proposed miRNAs adhere to previously observed characteristics and thus it is reasonable to suspect that these interactions would occur *in vivo*.

Findings of the ErbB2 and ErbB3 Transfections in M12+miR17-3p cells:

The M12+miR-17-3p cell line was transfected with the pErbB2 and pErbB3 plasmids to elucidate any potential miR17-3p interaction between the ErbB2 and ErbB3 3'UTRs in prostate cancer. Figure 4-7 depicts the results from the transfections of PGL3/Renilla, pErbB2/Renilla and pErbB3/Renilla in the M12+miR-17-3p cell line. If there was a direct interaction between miR17-3p and the ErbB2 and ErbB3 3'UTRs we would have expected a decrease in the ratio of firefly to renilla expression between PGL3 and the pErbBs. Based on these results, it was concluded that miR17-3p may be indirectly affecting the translation of the ErbB2 and ErbB3 mRNAs, but no direct binding within the 3'UTRs of pErbB2 or pErbB3 could be detected by this assay method.

Figure 4-7: miR17-3p does not directly affect luciferase expression of pErBb2 or pErbB3 in the M12+miR17-3p cell line.

M12+miR17-3p cells (200,000 cells per well) were transfected in triplicate with 1µg of PGL3

empty vector, pErbB2 or pErbB3 plasmids. Luciferase activity was measured 48 hrs later and

expressed as the ratio of firefly to renilla. Standard deviation within each sample is shown.

Figure 4-7: miR17-3p does not directly affect luciferase expression of pErBb2 or pErbB3 in the M12+miR17-3p cell line.
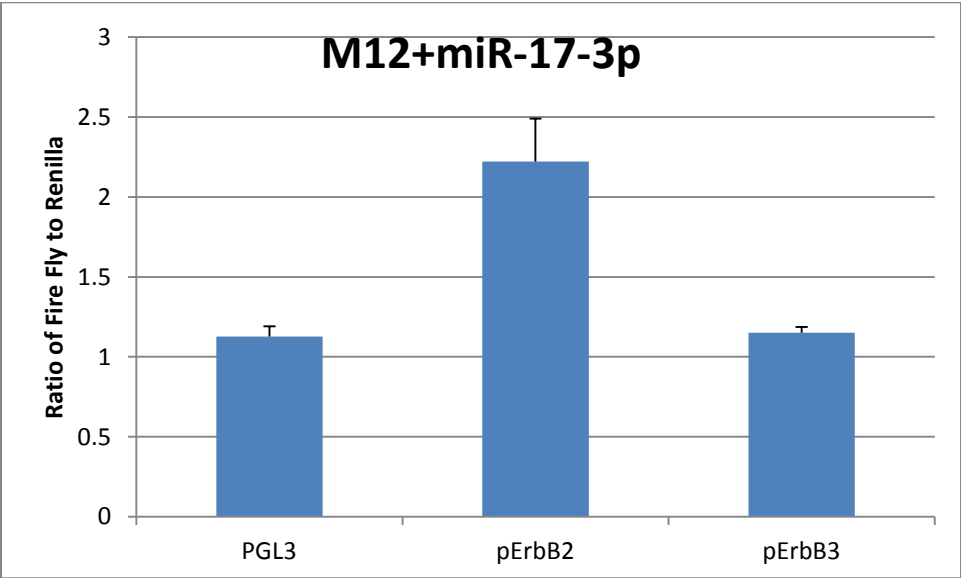
Discussion:

We took a multifaceted approach, combining a computationally built protein-protein interaction network of proteins experimentally proven to be targeted by miRNAs with high throughput proteomics to identify key protein targets in prostate cancer. This analysis coupled with screening the miRnome enhanced our identification of miRNAs that are dysregulated in prostate cancer. To our knowledge, this study is the first to combine all three approaches to elucidate new miRNAs and targets contributing to prostate cancer progression.

Our computational networks approach identified the ErbB family of proteins as highly connected nodes and therefore key players in the prostate cancer network. Additionally, proteomic analysis of our prostate cancer progression model suggested ErbB2 and ErbB3 as significantly dysregulated proteins. Several miRNA array screens substantiated by single miR analysis of the P69 and M12 related sublines produced miR125b as being highly differentially expressed. Previously, it was suggested that miR125b targets ErbB2 and ErbB3 and functions as a tumor suppressor in breast cancer [20]. Our results suggest a similar function for miR125b in prostate cancer where the differential expression of miR125b could be responsible at least in part for the dysregulation of the ErbBs.

Reporter gene assays were conducted to further explore the relationship between miR125b and the ErbBs. Fusion of the entire 3'UTR of either ErbB2 or ErbB3 to the luciferase reporter gene resulted in a 2.8-fold and 2.4-fold decrease (respectively) in activity in p69 cells compared to the parental PGL3 vector. However, inclusion of the miR125b/ErbB2 or ErbB3 binding sites as proposed in the Scott et al paper did not produce the luciferase expression profiles expected of a miRNA/target interaction [20]. Several theories could explain the inconsistency between our results and those previously published. Foremost is the fact that the

69

binding site identified in the Scott et al paper was not examined by mutagenesis and therefore may be incorrect. Recently, the National Institutes of Health published a manuscript describing experimental methods to most accurately validate miRNA targets [60]. Here, it was concluded that insertion of the entire 3'UTR of the target into the expression vector is necessary to prevent unintentional structural changes that may hinder miRNA/target binding. Thus, transfection of a plasmid containing the entire 3'UTR fused to a reporter compared to selected base pair mutations of just that region targeted by the miRNA seed within the entire 3'UTR is proposed to be a more accurate option to prove a miRNA/target interaction. In the case of the Scott et al paper [20], failure to specifically mutate just those bases proposed to be targeted by the seed region of miR125b fails to prove a specific miR125b interaction, yet numerous papers in the literature refer to this paper as proof of ErbB2 or ErbB3/miR125b interaction. However, many researchers have used this approach to presumably validate miRNA/mRNA interaction. We found that fusion of just the target region or a 3 base pair mutation thereof failed to produce any change in reporter activity. In agreement with NIH guidelines this could be due to the inability to correctly duplicate a structurally active target region [60]. Alternatively, it may be due to the fact that we mutated only 3 of the bases within the target region. It may be necessary to mutate all 6 bases within miR125b target site before ruling out the importance of this region as a functional miR125b binding site.

The aforementioned NIH guidelines go on to state that over-expression of the miRNA to increase miRNA copy availability is not necessary or "ideal" to validate miRNA/mRNA interaction because this could lead to non-physiological interactions [60]. When Scott et al performed their analysis, they infected their cells with a retrovius expressing a mature miR125b sequence to attain high level expression [20]. From the NIH guidelines this might not be the most

relevant protocol. In our case we used P69 cells which naturally express miR125b at a level significantly higher than the M12 cell line. Thus, we were not forced to artificially manipulate miR125b expression levels but rather worked within the confines of endogenous expression levels.

Lastly, deletion of ErbB2 (44 bp) or ErbB3's (22 bp) proposed miR125 binding site in the Scott et al paper, produced at best only a 1.4-fold decrease in luciferase activity compared to the wild type vector [20]. In our case inclusion of the entire 3'UTRs generated a significantly greater decrease, 2.4- or 2.8-fold, compared to the PGL3 vector with no insert. Our results suggest additional mechanisms of ErbB regulation above those included by the aforementioned deletions. The most obvious explanation here is that multiple miR125b binding sites might reside within the 3'UTRs of ErbB2 or ErbB3, which in a combinatorial fashion control ErbB expression. The contribution of only one of these sites, and maybe not the most functional site, was studied by Scoot et al. In fact, further computational examination of the ErbB2 and ErbB3 3'UTRs using RNAhybrid, identified a better miR125b binding site to ErB2[59]. Figure 4-8 depicts a potential structure formed with a lower minimum free energy of conformation (-24.4kcal/mol) than that exhibited by the Scott region (-21.9 kcal/mol). The structure of the proposed binding site adheres to previously observed characteristics and thus it is reasonable to suspect that this interaction would occur *in vivo*. Future experiments including mutation of these relevant seed region target bases will be required to determine if this is a functional miR125b binding site.

Last of all, it is possible that miRNAs in addition to or together with miR125b is targeting the ErbBs. Previously, single miRNA analysis showed that miR17-3p is differentially expressed in our prostate progression model. Additional experiments showed that miR17-3p can act as a tumor suppressor in vitro and in vivo [31]. Proteomic data showed that overexpressing

71

Figure 4-8: A better predicted miR125b binding site within the ErbB2 3'UTR.

RNAhybrid predicted structure of binding between miR125b and the 3' UTR of ErbB2 [59].

miR125b is represented in green and the 3'UTR of ErbB2 is represented in red.

Figure 4-8: Predicted best miR125b coupling with the ErbB2 3'UTR.

mfe: -24.4 kcal/mol
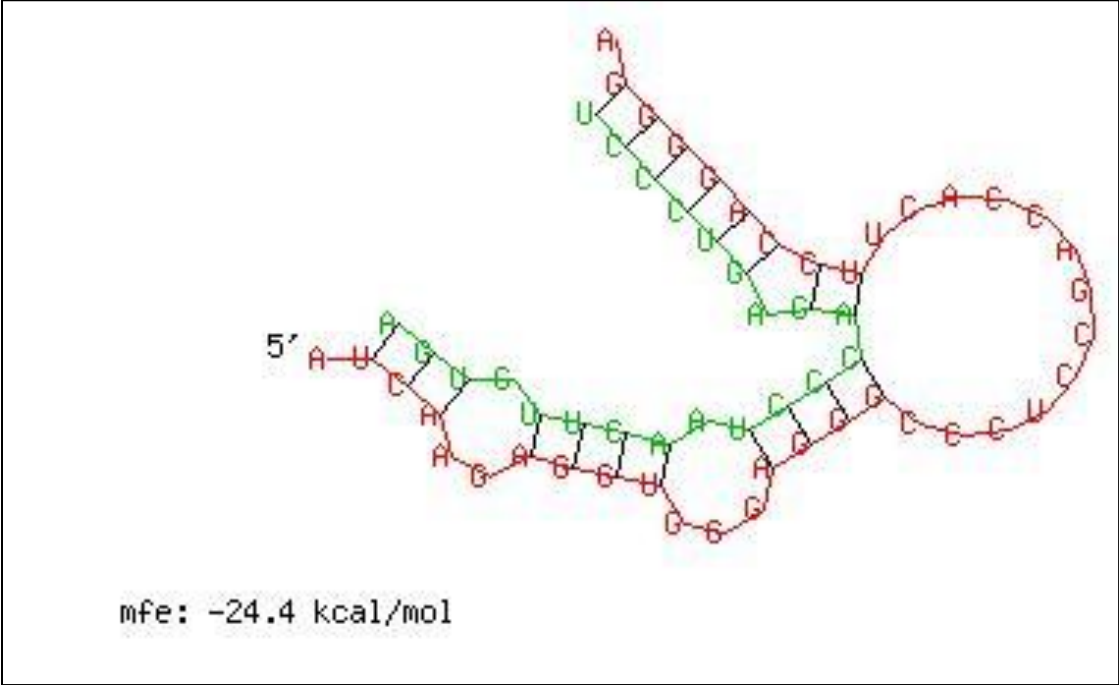
miR-17-3p in the M12 cell line resulted in a decrease in expression of ErbB2 and ErbB3 suggesting additional regulation by miR17-3p. However, luciferase assays did not confirm a direct interaction between miR17-3p binding and a predicted binding site within ErbB's 3'UTR. This suggests that miR17-3p is either binding to another unknown site or is affecting the expression of a secondary molecule which in turn affects ErbB2 or ErbB3 expression. Although miR17-3p's direct interaction on the ErbBs could not be confirmed as yet, our miR screen analysis does suggest many miRs that are differentially expressed in the various cell lines of our cancer progression model. Thus, there is a strong possibility that additional miRNAs targeting the ErbBs will be uncovered in the continuation of these studies.

In summary the compilation of results from a computational networks approach, proteomics and miRnome analysis has suggested miR125b and the ErbBs as relevant players in prostate cancer progression. Potentially new miRNAs and targets have thus been identified, which warrant further study. Prostate cancer is the second most common cancer affecting men today and the second leading cause of cancer deaths in American men. Therefore, there is a strong need for accurate biomarkers and successful therapeutic treatments in which identification of miRNAs and proteins that contribute to prostate cancer progression could prove invaluable to combating this disease.

References

1. http://www.cancer.org/acs/groups/content/@epidemiologysurveilance/documents/document/acspc-031941.pdf.

2. Jathal, M. K., Chen, L., Mudryj, M. & Ghosh, P. M. Targeting ErbB3: the New RTK(id) on the Prostate Cancer Block. *Immunol. Endocr Metab. Agents Med. Chem.* 11, 131-149 (2011).

3. SEER*Stat Database: Incidence - SEER 9 Regs Research Data, Nov 2011 Sub (1973-2009) (2011).

4. http://apps.nccd.cdc.gov/uscs/.

5. Hankey, B. F. *et al*. Cancer surveillance series: interpreting trends in prostate cancer--part I: Evidence of the effects of screening in recent prostate cancer incidence, mortality, and survival rates. *J. Natl. Cancer Inst.* 91, 1017-1024 (1999).

6. http://www.cancer.gov/cancertopics/types/prostate.

7. Catalona, W. J. *et al*. Comparison of digital rectal examination and serum prostate specific antigen in the early detection of prostate cancer: results of a multicenter clinical trial of 6,630 men. *J. Urol.* 151, 1283-1290 (1994).

8. Xie, B. X. *et al*. Analysis of differentially expressed genes in LNCaP prostate cancer progression model. *J. Androl.* 32, 170-182 (2011).

9. Taplin, M. E. *et al*. Mutation of the androgen-receptor gene in metastatic androgen-independent prostate cancer. *N. Engl. J. Med.* 332, 1393-1398 (1995).

10. Fabbri, M., Croce, C. M. & Calin, G. A. MicroRNAs. *Cancer J.* 14, 1-6 (2008).

11. Griffiths-Jones, S., Saini, H. K., van Dongen, S. & Enright, A. J. miRBase: tools for microRNA genomics. *Nucleic Acids Res.* 36, D154-8 (2008).

12. Li, M., Li, J., Ding, X., He, M. & Cheng, S. Y. microRNA and cancer. *AAPS J.* 12, 309-317 (2010).

13. Lee, Y., Jeon, K., Lee, J. T., Kim, S. & Kim, V. N. MicroRNA maturation: stepwise processing and subcellular localization. *EMBO J.* 21, 4663-4670 (2002).

14. Olena, A. F. & Patton, J. G. Genomic organization of microRNAs. *J. Cell. Physiol.* 222, 540-545 (2010).

15. Lytle, J. R., Yario, T. A. & Steitz, J. A. Target mRNAs are repressed as efficiently by microRNA-binding sites in the 5' UTR as in the 3' UTR. *Proc. Natl. Acad. Sci. U. S. A.* 104, 9667-9672 (2007).

16. O'Donnell, K. A., Wentzel, E. A., Zeller, K. I., Dang, C. V. & Mendell, J. T. c-Myc-regulated microRNAs modulate E2F1 expression. *Nature* 435, 839-843 (2005).

17. Mendell, J. T. miRiad roles for the miR-17-92 cluster in development and disease. *Cell* 133, 217-222 (2008).

18. Volinia, S. *et al*. A microRNA expression signature of human solid tumors defines cancer gene targets. *Proc. Natl. Acad. Sci. U. S. A.* 103, 2257-2261 (2006).

19. Zhang, X. *et al*. MicroRNA-17-3p is a prostate tumor suppressor in vitro and in vivo, and is decreased in high grade prostate tumors analyzed by laser capture microdissection. *Clin. Exp. Metastasis* 26, 965-979 (2009).

20. Scott, G. K. *et al*. Coordinate suppression of ERBB2 and ERBB3 by enforced expression of micro-RNA miR-125a or miR-125b. *J. Biol. Chem.* 282, 1479-1486 (2007).

21. Baffa, R. *et al*. MicroRNA expression profiling of human metastatic cancers identifies cancer gene targets. *J. Pathol.* 219, 214-221 (2009).

22. Yang, H. *et al*. MicroRNA expression profiling in human ovarian cancer: miR-214 induces cell survival and cisplatin resistance by targeting PTEN. *Cancer Res.* 68, 425-433 (2008).

23. Wong, T. S. *et al*. Mature miR-184 as Potential Oncogenic microRNA of Squamous Cell Carcinoma of Tongue. *Clin. Cancer Res.* 14, 2588-2592 (2008).

24. Laneve, P. *et al*. The interplay between microRNAs and the neurotrophin receptor tropomyosin-related kinase C controls proliferation of human neuroblastoma cells. *Proc. Natl. Acad. Sci. U. S. A.* 104, 7957-7962 (2007).

25. Ueda, T. *et al*. Relation between microRNA expression and progression and prognosis of gastric cancer: a microRNA expression analysis. *Lancet Oncol.* 11, 136-146 (2010).

26. Veerla, S. *et al*. MiRNA expression in urothelial carcinomas: important roles of miR-10a, miR-222, miR-125b, miR-7 and miR-452 for tumor stage and metastasis, and frequent homozygous losses of miR-31. *Int. J. Cancer* 124, 2236-2242 (2009).

27. Xiao, F. *et al*. miRecords: an integrated resource for microRNA-target interactions. *Nucleic Acids Res.* 37, D105-10 (2009).

28. Sobel, R. E. & Sadar, M. D. Cell lines used in prostate cancer research: a compendium of old and new lines--part 1. *J. Urol.* 173, 342-359 (2005).

29. Bae, V. L. *et al*. Metastatic sublines of an SV40 large T antigen immortalized human prostate epithelial cell line. *Prostate* 34, 275-282 (1998).

30. Astbury, C., Jackson-Cook, C. K., Culp, S. H., Paisley, T. E. & Ware, J. L. Suppression of tumorigenicity in the human prostate cancer cell line M12 via microcell-mediated restoration of chromosome 19. *Genes Chromosomes Cancer* 31, 143-155 (2001).

31. Zhang, X. *et al*. MicroRNA-17-3p is a prostate tumor suppressor in vitro and in vivo, and is decreased in high grade prostate tumors analyzed by laser capture microdissection. *Clin. Exp. Metastasis* 26, 965-979 (2009).

32. Olayioye, M. A., Neve, R. M., Lane, H. A. & Hynes, N. E. The ErbB signaling network: receptor heterodimerization in development and cancer. *EMBO J.* 19, 3159-3167 (2000).

33. Grasso, A. W. *et al*. ErbB kinases and NDF signaling in human prostate cancer cells. *Oncogene* 15, 2705-2716 (1997).

34. Lorenzo, G. D., Bianco, R., Tortora, G. & Ciardiello, F. Involvement of growth factor receptors of the epidermal growth factor receptor family in prostate cancer development and progression to androgen independence. *Clin. Prostate Cancer.* 2, 50-57 (2003).

35. Gioeli, D., Mandell, J. W., Petroni, G. R., Frierson, H. F.,Jr & Weber, M. J. Activation of mitogen-activated protein kinase associated with prostate cancer progression. *Cancer Res.* 59, 279-284 (1999).

36. Lu, X. & Kang, Y. Epidermal growth factor signalling and bone metastasis. *Br. J. Cancer* 102, 457-461 (2010).

37. Holbro, T. *et al*. The ErbB2/ErbB3 heterodimer functions as an oncogenic unit: ErbB2 requires ErbB3 to drive breast tumor cell proliferation. *Proc. Natl. Acad. Sci. U. S. A.* 100, 8933-8938 (2003).

38. Chen, L. *et al*. Nrdp1-mediated regulation of ErbB3 expression by the androgen receptor in androgen-dependent but not castrate-resistant prostate cancer cells. *Cancer Res.* 70, 5994-6003 (2010).

39. Cho, W. C. MicroRNAs: potential biomarkers for cancer diagnosis, prognosis and targets for therapy. *Int. J. Biochem. Cell Biol.* 42, 1273-1281 (2010).

40. Singh, D. *et al*. Gene expression correlates of clinical prostate cancer behavior. *Cancer. Cell.* 1, 203-209 (2002).

41. Sheehan, K. M. *et al*. Use of reverse phase protein microarrays and reference standard development for molecular network analysis of metastatic ovarian carcinoma. *Mol. Cell. Proteomics* 4, 346-355 (2005).

42. Pavlickova, P., Schneider, E. M. & Hug, H. Advances in recombinant antibody microarrays. *Clin. Chim. Acta* 343, 17-35 (2004).

43. Paweletz, C. P. *et al*. Reverse phase protein microarrays which capture disease progression show activation of pro-survival pathways at the cancer invasion front. *Oncogene* 20, 1981-1989 (2001).

44. Tibes, R. *et al*. Reverse phase protein array: validation of a novel proteomic technology and utility for analysis of primary leukemia specimens and hematopoietic stem cells. *Mol. Cancer. Ther.* 5, 2512-2521 (2006).

45. Nishizuka, S. *et al*. Proteomic profiling of the NCI-60 cancer cell lines using new high-density reverse-phase lysate microarrays. *Proc. Natl. Acad. Sci. U. S. A*. 100, 14229-14234 (2003).

46. Zhu, X., Gerstein, M. & Snyder, M. Getting connected: analysis and principles of biological networks. *Genes Dev.* 21, 1010-1024 (2007).

47. Yook, S. H., Oltvai, Z. N. & Barabasi, A. L. Functional and topological characterization of protein interaction networks. *Proteomics* 4, 928-942 (2004).

48. Jiang, Q. *et al*. miR2Disease: a manually curated database for microRNA deregulation in human disease. *Nucleic Acids Res.* 37, D98-104 (2009).

49. Papadopoulos, G. L., Reczko, M., Simossis, V. A., Sethupathy, P. & Hatzigeorgiou, A. G. The database of experimentally supported targets: a functional update of TarBase. *Nucleic Acids Res.* 37, D155-8 (2009).

50. Boguski, M. S. & Schuler, G. D. ESTablishing a human transcript map. *Nat. Genet.* 10, 369-371 (1995).

51. Cline, M. S. *et al*. Integration of biological networks and gene expression data using Cytoscape. *Nat. Protoc.* 2, 2366-2382 (2007).

52. Vailaya, A. *et al*. An architecture for biological information extraction and representation. *Bioinformatics* 21, 430-438 (2005).

53. Scardoni, G., Petterlini, M. & Laudanna, C. Analyzing biological network parameters with CentiScaPe. *Bioinformatics* 25, 2857-2859 (2009).

54. Budd, W. T., Weaver, D. E., Anderson, J. & Zehner, Z. E. MicroRNA Dysregulation in Prostate Cancer: Network Analysis Reveals Preferential Regulation of Highly Connected Nodes. *Chemistry & Biodiversity* 9 (2012 (In Press)).

55. Batada, N. N., Hurst, L. D. & Tyers, M. Evolutionary and physiological importance of hub proteins. *PLoS Comput. Biol.* 2, e88 (2006).

56. Liang, H. & Li, W. H. Gene essentiality, gene duplicability and protein connectivity in human and mouse. *Trends Genet.* 23, 375-378 (2007).

57. Pruitt, K. D., Tatusova, T. & Maglott, D. R. NCBI reference sequences (RefSeq): a curated non-redundant sequence database of genomes, transcripts and proteins. *Nucleic Acids Res.* 35, D61-5 (2007).

58. Kozomara, A. & Griffiths-Jones, S. miRBase: integrating microRNA annotation and deep-sequencing data. *Nucleic Acids Res.* 39, D152-7 (2011).

59. Rehmsmeier, M., Steffen, P., Hochsmann, M. & Giegerich, R. Fast and effective prediction of microRNA/target duplexes. *RNA* 10, 1507-1517 (2004).

60. Kuhn, D. E. *et al*. Experimental validation of miRNA targets. *Methods* 44, 47-54 (2008).

Vita

Danielle Elizabeth Weaver was born on September 29, 1987, in Fairfax County, Virginia, and is

an American citizen. She graduated from Osbourn Park High School, Manassas, Virginia in

2005. She received her Bachelor of Science in Forensic Science from Virginia Commonwealth

University, Richmond, Virginia in 2009. She has taught Introduction to Life Sciences at Virginia

Commonwealth University during the pursuit of her graduate degree.